Journal of Catalysis 410 (2022) 206–220

Contents lists available at ScienceDirect

Journal of Catalysis

journal homepage: www.elsevier.com/locate/jcat

Synthesis, characterization, and function of Au nanoparticles within TS-1 zeotypes as catalysts for alkene epoxidation using O_2/H_2O reactants

Trenton Otto [a,b], Xiaoyu Zhou [a,c], Stacey I. Zones [d], Enrique Iglesia [a,*]

[a] Department of Chemical and Biomolecular Engineering, University of California at Berkeley, Berkeley, CA 94720, USA
[b] Chevron Energy Technology Company, Richmond, CA 94804, USA[1]
[c] Department of Chemistry, Technical University of Munich, 85748 Munich, Germany[1]
[d] Chevron Energy Technology Company, Richmond, CA 94804, USA

ARTICLE INFO

Article history:
Received 26 February 2022
Revised 1 April 2022
Accepted 4 April 2022
Available online 11 April 2022

Keywords:
Gold catalyst
Metal encapsulation
Propylene epoxidation
Silicalite-1
Bifunctional catalyst
Titanium
Hydrothermal synthesis

ABSTRACT

A synthetic procedure was developed for the encapsulation of Au nanoparticles within titanium silicalite-1 (TS-1). Encapsulation was achieved via crystallization of TS-1 synthesis gels containing ligated Au cations, resulting in TS-1 framework assembly around Au coordination complexes. X-Ray diffraction and micropore volume measurements indicated that TS-1 could be crystallized at much milder conditions than previously reported, allowing the assembly of TS-1 without concomitant decomposition of added Au complexes. Infrared (IR) and UV–vis spectroscopy showed that Ti was incorporated into the frameworks as tetrahedrally coordinated atoms. Changes to established crystallization procedures for TS-1 included lower temperature (393 K vs. 448 K) compensated by longer time (120 vs 48 h) and the use of seed crystals. Post-synthetic thermal treatments led to the formation of small Au nanoparticles (2.8–3.8 nm) visible in electron micrographs and free of organic debris, as indicated by IR spectroscopy. Such nanoparticles are protected from bulky titrants, and thus reside within TS-1 crystallites (>96% encapsulation). The Au particles were active for propene epoxidation with H_2O/O_2 even without promotion by alkali cations (e.g., Cs^+), though alkali doping led to enhanced rates. These Au/TS-1 systems were less active for epoxidation than Au/TS-1 prepared by deposition–precipitation, likely because the latter contains a disproportionately active minority population of exceedingly small (<1 nm) Au clusters.

1. Introduction

Au nanoparticles have attracted considerable attention because of their potential catalytic applications for a broad range of reactions, including CO oxidation, alkanol oxidation, and selective diene hydrogenation [1–3]. Highly-dispersed (<5 nm) Au nanoparticles deposited on amorphous or crystalline oxides containing Ti atoms (e.g., TiO_2 and titanium-containing silicalite-1 (TS-1)) also catalyze alkene epoxidation using O_2 as the oxidant [3–6]. Au/Ti-oxide catalysts for propylene epoxidation are of specific practical interest because propylene oxide (PO) is an intermediate in the synthesis of polyether polyols, propylene glycol, and several other chemicals [7]. Propylene epoxidation occurs on Au/Ti-oxide compounds in the presence of H_2/O_2 mixtures, which have been proposed to form H_2O_2 on Au surfaces and then react with propylene at Ti centers present within molecular distances via the formation of hydroperoxy (*OOH) [7,8] or bound hydrogen peroxide (*HOOH) species [9] and epoxidation events analogous to those on TS-1 with propylene-H_2O_2 co-reactants [3,4]. These hydroperoxy species are also thought to form on Au surfaces from H_2O/O_2 reactant mixtures, albeit with much less favorable thermodynamics [10–12]. For both H_2/O_2 and H_2O/O_2 reactants, epoxidation rates and selectivities seem to depend sensitively on the proximity between the Au and the Ti function [8–12], apparently because highly-reactive intermediates must be shuttled between Au and Ti domains. Such expected benefits of intimacy have led to significant efforts to develop protocols for the synthesis of solids with more proximate Au and Ti functions. These methods typically seek to place small Au nanoparticles within (or at the external surfaces of) TS-1 crystals; TS-1 is the preferred epoxidation function because it contains highly dispersed Ti centers with the tetrahedral coordination shown to be most effective for alkene-H_2O_2 reactions [4,8,11,12].

Au nanoparticles 2–4 nm in diameter can be deposited at external TS-1 surfaces via deposition–precipitation (DP) methods using Na_2CO_3 [13–15], K_2CO_3 [16], or Cs_2CO_3 [16] as the precipitant of $HAuCl_4$ precursors. These procedures lead to some of the most

* Corresponding author at: University of California, Berkeley, 103 Gilman Hall, Berkeley, CA 94720-1462, USA
E-mail address: iglesia@berkeley.edu (E. Iglesia).
[1] Current address.

https://doi.org/10.1016/j.jcat.2022.04.002
0021-9517/

active and selective Au/TS-1 catalysts for propylene epoxidation with both H_2/O_2 and H_2O/O_2 co-reactants [11,13–16], even though the detectable Au-containing nanoparticles are predominantly located at the external surfaces of TS-1 crystallites. Density functional theory (DFT) [17] calculations have suggested that propylene epoxidation with H_2/O_2 is most favorable on Ti sites that reside within atomic contact of very small (<1 nm) Au nanoparticles [17], but the presence and involvement of such contact have resisted direct experimental observation.

Catalysts prepared by deposition of Au nanoparticles on silicalite-coated TS-1 (Au/S-1/TS-1) and on uncoated TS-1 (Au/TS-1) showed similar activity for propylene epoxidation, suggesting that a small fraction of highly dispersed (<1 nm) Au clusters, present within TS-1 crystals instead of at external surfaces (where Au-Ti contact is precluded in Au/S-1/TS-1) may account for most of the observed epoxidation turnovers on Au/TS-1 [18]. DP methods that form Au nanoparticles with the small diameter required for high reactivity (<5 nm [19]) are limited to very low Au contents (<0.35% wt. [11]); they form only when a small fraction (<5%) of the Au^{3+} species in the aqueous solutions are precipitated and deposited [11]. Mechanical grinding of solids [20] have also been used to form small (<2 nm) Au clusters at external TS-1 surfaces, albeit at very low Au contents (<0.30% wt.). AuPd particles (∼2 nm) can be dispersed within mesopores in hierarchical TS-1 samples (prepared by crystallization of protozeolitic precursors) via post-synthetic impregnation and thermal treatment of Au^{3+} and Pd^{2+} precursors [21]. Benzyl alcohol oxidation rates measured (per mass) in the presence of H_2/O_2 mixtures (to form H_2O_2 in-situ) on these AuPd catalysts were higher than on samples with larger AuPd particles derived from DP protocols on hierarchical TS-1 [21]. To the best of our knowledge, these methods represent the current state-of-the-art for the synthesis of H_2O_2 or OOH-generating Au functions within short distances (but larger than atomic and molecular dimensions) of Ti centers within TS-1.

The present study reports a synthetic strategy for the direct encapsulation of Au nanoparticles within TS-1 crystals during the hydrothermal synthesis of such crystalline microporous solids. These protocols place the Au and Ti functions within short intervening distances. Such materials cannot be prepared by post-synthetic exchange of solvated Au^{3+} precursors followed by thermal treatment [22] because TS-1 lacks cation exchange sites, and also because its ten member-ring (10-MR) apertures obstruct the diffusion of aqueous Au^{3+} cations and their coordinating sphere into intracrystalline regions [23]. The protocols reported here involve the hydrothermal assembly of TS-1 zeotype frameworks around ligand-protected Au^{3+} cations to form coordination complexes that are occluded within TS-1 voids during crystallization. Subsequent thermal treatments then remove ligand species, leading to the formation of small and stable nanoparticles that predominantly reside within intracrystalline voids. These methods represent a significant extension of protocols developed previously for several other metals and zeotypes (LTA, MFI, FAU, GIS, ANA, SOD, CHA; [24–28]) to the synthesis of Au nanoparticles for the specific case of TS-1 and SIL structures that lack exchange sites and require organic templates and higher temperatures than other structures for their crystallization under hydrothermal conditions.

These encapsulation methods are singularly challenging for Au cations, because of their propensity to reduce prematurely and form large Au^0 colloids before the nucleation and growth of the confining crystalline frameworks [23]. These challenges are formidable for TS-1, in particular, because the temperatures required for TS-1 crystallization (∼450 K; [29,30]) are higher than for the aluminosilicates previously used in developing encapsulation protocols (e.g., LTA, MFI; 373–393 K; [23,24]). Such high temperatures favor the deprotection of ligated precursors and cause their premature precipitation or reduction during the assembly of zeotype frameworks [23,31,32]. The challenges imposed by these high synthesis temperatures and by the facile reduction of Au^{3+} compared with other noble metal cations [33], especially when alkanols formed by the hydrolysis of Si and Ti alkoxides act as chemical reductants [23], have prevented the synthesis of Au nanoparticles selectively dispersed within TS-1 until the present work.

These synthetic hurdles are circumvented here by (i) using 3-mercaptopropyl-trimethoxysilane (MPS) ligands that simultaneously protect Au^{3+} cations and enforce metal incorporation into proto-zeolitic moieties via their alkoxysilane groups; (ii) removing the alkanol reductants formed by alkoxide hydrolysis before contact between synthesis gels and ligated precursors; and (iii) crystallizing synthesis gels at moderate temperatures that prevent the premature reduction of Au^{3+} cations without compromising framework crystallization. These successful syntheses exploited TS-1 crystallization temperatures that are significantly lower than those in previous reports (393 K vs. 443–448 K; [29,30]), compensated by longer synthesis times (120 h vs. 48 h) and by the purposeful addition of small amounts of TS-1 seed crystals. These procedures led to Au/TS-1 materials with high crystallinity and solids yields and with Ti centers located within the silicate framework for a broad range of relevant Au contents (0.2–0.9% wt.).

Post-synthetic pyrolytic, oxidative, and reductive treatments successfully removed the ligands and organic templates and led to formation of 2.8–3.8 nm Au nanoparticles uniform in diameter and located within TS-1 crystals. Their formation required the partial decomposition of ligand and template species in inert environments and the gradual oxidative removal of organic residues in order to prevent local exotherms. The surface cleanliness of the confined Au nanoparticles was confirmed by infrared spectra of chemisorbed CO. Au particles were predominantly present within TS-1 voids (>96% of exposed Au surfaces), as shown from ethanol oxidative dehydrogenation (ODH) reaction rates on Au/TS-1 before and after exposure to dibenzothiophene (DBT), which poisons Au surfaces but cannot enter TS-1 voids.

Preliminary studies of propylene epoxidation with H_2O/O_2 indicate that the Au/TS-1 catalysts containing encapsulated Au particles are active for the formation of PO, with acrolein and propanal generated as the main byproducts. Au/TS-1 samples prepared with relatively small Au nanoparticles (∼2.8 nm) gave PO formation rates about 10-fold higher than for samples with larger particles (∼3.8 nm). These Au/TS-1 catalysts were active for PO formation despite the substantive absence (<1 ppm) of alkali (Cs^+, K^+) promoters, which were previously deemed essential to form PO on Au/TS-1 systems [11]. The deliberate post-synthesis addition of Cs species to Au/TS-1 samples led to about a two-fold increase in PO formation rates, but alkali-free samples were also competent in PO synthesis. PO formation rates and selectivites on both neat and alkali-promoted Au/TS-1 samples developed in this work, however, were lower than previously reported for Au/TS-1 systems prepared by DP methods with alkali promoters [11]. The presence of a population of exceedingly small (<1 nm) and difficult to detect Au clusters present in the Au/TS-1 samples prepared by DP methods, which utilize significantly lower treatment temperatures than the synthetic techniques used in this study, may account for the large observed discrepancy in PO formation rates on the two Au/TS-1 samples given the substantial Au particle size effect on the reaction rate.

2. Methods

2.1. Source and purity of reagents used

Distilled and deionized H_2O (17.9 Ω cm resistivity) was used in all syntheses. $HAuCl_4 \cdot 3H_2O$ (99.99%, Sigma-Aldrich), 40% wt.

tetrapropylammonium hydroxide (TPAOH) in H_2O (99% purity; Sigma-Aldrich), tetraethyl orthosilicate (TEOS; 98%, Sigma-Aldrich), tetraethyl orthotitanate (TEOT; 98%, Sigma-Aldrich), 3-mercaptopropyl-trimethoxysilane (95%, Sigma-Aldrich), Cs_2CO_3 (99.9%, Sigma-Aldrich), ethanol (99.9%, Sigma-Aldrich), dibenzothiophene (DBT; 98%, Sigma-Aldrich), propylene oxide (99%, Sigma-Aldrich), acetone (99.9%, Sigma-Aldrich), acrolein (99.9%, Sigma-Aldrich), isopropanol (99.9%, Sigma-Aldrich), propanal (99.9%, Sigma-Aldrich), fumed SiO_2 (Cab-O-Sil M5, >98.5%), quartz (Fluka, acid purified, product #84880, >99%), $BaSO_4$ (>99%, Sigma-Aldrich), 5–50% propylene/He (99.999%, Praxair), 20–25% O_2/He (99.999%, Praxair), air (extra dry; 99.999%, Praxair), H_2 (99.999%, Praxair), 1% CO/He (99.999%, Praxair), and He (99.999%, Praxair) were used as received.

2.2. Synthesis of TS-1 frameworks with ligated Au precursors in product crystals

The synthesis of Au/TS-1 was carried out using a modified version of the International Zeolite Association (IZA) recommended procedure [29] for TS-1 synthesis ($Ti_{1.3}Si_{94.7}O_{192}$) by introducing Au^{3+} cations (from $HAuCl_4$) protected by 3-mercaptopropyl-trimethoxysilane (MPS) ligands into TS-1 synthesis gels. The modifications were substantial and included not only the presence of the ligated Au^{3+} species, but also much longer synthesis times, lower temperatures, the full removal of alkanol reductants formed by the hydrolysis of Si and Ti precursors, and the use of seed crystals to promote crystallization at the milder conditions required to avoid the reduction of the ligated Au cations. These modified procedures lead to the successful crystallization of TS-1 frameworks at temperatures (393 K) significantly below those required in previously reported protocols (448 K; [29]).

The Au/TS-1 synthesis gels were prepared by placing tetraethyl orthosilicate (TEOS; 19.2 g) and tetraethyl orthotitanate (TEOT; 0.354 g) in a sealed polypropylene bottle and heating at 308 K for 0.5 h under magnetic stirring (6.7 Hz). This TEOS/TEOT mixture was cooled to 273 K in an ice bath and added dropwise (0.02 cm^3 s^{-1}) via graduated pipettes to 20 g of 40% wt. aqueous tetrapropyl ammonium hydroxide (TPAOH) also kept at 273 K while magnetically stirring at 6.7 Hz. The resulting mixture was heated to 358 K (at 0.067 K s^{-1}) for 4 h while stirring (6.7 Hz) in an open polypropylene bottle to allow the partial evaporation of the liquid. This step removes some water and most of the ethanol molecules formed upon hydrolysis of TEOS and TEOT. Ethanol decreases the solubility of silicate precursors during crystallization [29]; most importantly in this case, it also acts as a reductant for Au cations at synthesis temperatures [23]. One-half of the evaporated volume (after heating at 358 K for 4 h) was replaced with an aqueous solution of the MPS ligand (0.077–0.387 g in ~12 cm^3 H_2O). This mixture was homogenized at ambient temperature by stirring (6.7 Hz) and the remaining volume that was removed by evaporation (~12 cm^3) was replaced by dropwise addition of an aqueous solution of $HAuCl_4{\cdot}3H_2O$ (0.02–0.11 g), followed by heating to 358 K (at 0.067 K s^{-1}) for 4 h while stirring (6.7 Hz) in an open bottle. Deionized H_2O was periodically added to the solution during this second evaporation process in order to maintain a constant liquid volume. These procedures led to homogeneous Au/TS-1 synthesis gels with molar ratios of 1 TiO_2:70 SiO_2:1980 H_2O:30 TPAOH:0.30–1.49 ligand:0.043–0.213 Au.

Batches of Au/TS-1 synthesis gels were crystallized within Teflon-lined stainless steel autoclaves by heating them at 0.067 K s^{-1} (while tumbling at 1.7 Hz) to a temperature between 393 and 448 K for periods between 48 and 120 h. Au/TS-1 solids were isolated by centrifugation (Sorvall RC-6 plus, 133 Hz) and settled and re-suspended with fresh deionized water (7–8 repetitions, ~50 cm^3 g^{-1}) several times until the suspending liquids in centrifuge tubes reached a pH of 7–8; isolated and washed samples were treated for 8 h at 373 K in a pre-heated convection oven containing ambient air. Different crystallization times and temperatures were examined in order to identify synthesis conditions that formed crystalline TS-1 without the premature reduction of Au cations and the formation of colloidal Au, as determined by the presence or absence of Au particles visible in the electron micrographs of the as-synthesized samples.

In some tests, TS-1 seeds (0.55 g) were added to Au/TS-1 synthesis gels before heating and crystallization. The seed crystals were prepared using the above procedures, but with crystallization at 448 K for 48 h and without the presence of ligands or Au precursors. The amount of seed crystals added (0.55 g) corresponds to 10% wt. of the solids that would have formed from the complete crystallization of the starting gel at 448 K for 48 h and in the absence of added Au^{3+} or MPS ligands. The Au content in most tests was chosen to form Au/TS-1 samples with about 1% wt. Au. Samples were also synthesized with lower Au loadings (~0.2% wt. nominal Au).

Procedures that led to the assembly of crystalline TS-1 without the premature reduction of Au^{3+} species were determined based on synthesis experiments conducted at a variety of conditions (Section 3.1); such procedures entailed the crystallization of Au/TS-1 synthesis gels in the presence of 10% wt. seed crystals at 393 K for 120 h. The temperature used (393 K) is about 50 K lower than in previously reported TS-1 synthesis protocols; such temperatures prevented the reduction and decomposition of ligated Au precursors and the premature formation of Au colloids, which cannot be encapsulated within TS-1 crystals because of their size, caused by their extensive agglomeration before the nucleation of the crystalline frameworks.

2.3. Post-synthetic thermal treatments and alkali doping of as-synthesized Au/TS-1

Post-synthetic thermal treatments were used in order to remove organic templates and ligands from as-synthesized Au/TS-1 and to form small encapsulated Au nanoparticles. The oxidative removal of organic templates from zeotype crystals typically leads to local exotherms that can sinter occluded Au species [23], thus requiring staged thermal treatments to remove these organic species in a controlled manner [23]. Organic compounds confined within zeotype crystals can also be partially removed using thermal treatments in an inert environment, which causes instead their endothermic pyrolysis.

The size and surface cleanliness (Section 2.4) of the Au nanoparticles formed after specific thermal treatment protocols were examined in order to develop procedures that fully removed synthetic residues from Au surfaces without concomitant formation of large (>5 nm) Au aggregates. These systematic studies led to thermal treatment procedures in which Au/TS-1 samples were heated (at 0.017 K s^{-1} in all cases) in either air or via sequential treatments in He and then in air (at 1.67 cm^3 g^{-1} s^{-1} in all cases) for periods of 2 h each at different temperatures between 448 K and 723 K. Each procedure ended with a treatment in air at 773 K for 2 h and subsequent exposure to H_2 (1.67 cm^3 g^{-1} s^{-1}) at 723 K for 2 h. Detailed diagrams of these thermal treatment protocols are shown in Section S1 (air treatment alone) and S2 (sequential He and air treatment) of the Supporting Information (SI).

A portion of the thermally treated Au/TS-1 samples were doped with Cs species, via incipient-wetness impregnation by aqueous Cs_2CO_3, prior to their use in propene epoxidation experiments (Section 2.5.2). Impregnation was carried out at ambient conditions using liquid solutions containing dissolved Cs_2CO_3 in quantities leading to nominal Cs/Au molar ratios of either 7 or 12. Alkali-impregnated samples were additionally treated in ambi-

ent air for 12 h at 373 K prior to their use in any reaction experiments.

2.4. Characterization of TS-1 phase purity and Ti speciation and of Au nanoparticle size and surface cleanliness

X-Ray diffractograms (XRD) were used to measure TS-1 crystallinity using a D8 Discover GADDS Powder Diffractometer with Cu-Kα radiation (λ = 0.15418 nm, 40 kV, 40 mA; 2θ = 5-50°; 0.00625°s^{-1} scan rate) and finely-ground solids dispersed onto quartz slides. The diffractogram for metal-free TS-1 (prepared via the IZA method [29]; Section 2.2) was used as a standard to determine the crystallinity of all Au/TS-1 samples, based on the integrated intensities of the three strongest diffraction lines in TS-1 (2θ: 23.2°, 23.9°, 24.4°).

Transmission electron microscopy (TEM) was used to determine the diameter of Au nanoparticles in each Au/TS-1 sample. Samples were prepared for TEM analysis by grinding them into a fine powder, suspending the solids in liquid acetone, and spreading the suspension onto holey carbon films mounted on 400 mesh copper grids (Ted Pella Inc.). A Philips/FEI Technai 12 microscope operating at 120 kV was used to collect the electron micrographs. Au particle sizes were measured based on the micrograph images and then used to calculate surface-averaged diameters ($\langle d_{TEM}\rangle$) [25]:

$$\langle d_{TEM}\rangle = \frac{\sum n_i d_i^3}{\sum n_i d_i^2} \quad (1)$$

where n_i is the number of particles with diameter d_i. The Au dispersion (defined as the fraction of Au atoms that reside at particle surfaces; D) was estimated from $\langle d_{TEM}\rangle$ values [34]:

$$D = 6\frac{v_m/a_m}{\langle d_{TEM}\rangle} \quad (2)$$

where a_m is the area occupied by an Au atom (8.75×10^{-2} nm^2) on a polycrystalline Au surface and v_m is the bulk atomic volume of Au (16.49×10^{-3} nm^3) [35]. Au particle diameters were also used to calculate number-averaged diameters ($\langle d_n\rangle$) and dispersity indices (DI) [25]:

$$DI = \frac{\langle d_{TEM}\rangle}{\langle d_n\rangle} = \frac{\left(\frac{\sum n_i d_i^3}{\sum n_i d_i^2}\right)}{\left(\frac{\sum n_i d_i}{\sum n_i}\right)} \quad (3)$$

These DI values represent the accepted IUPAC metric of size uniformity, with samples having values smaller than 1.5 considered to be essentially monodisperse [34].

The micropore volume of TS-1 and Au/TS-1 samples was estimated via CO_2 adsorption measurements (0–107 kPa CO_2) at 273 K using a Micromeritics 3Flex Surface Characterization Analyzer; micropore volumes were calculated from CO_2 uptakes using the Dubinin-Astakhov method [36]. Samples (~0.5 g) were heated at a rate of 0.17 K s^{-1} to 623 K under vacuum and held for a period of 4 h before CO_2 uptake measurements. CO_2 was used as the adsorbed probe molecule at 273 K (instead of N_2 at 77 K) because N_2 diffusion is very slow at 77 K (to achieve equivalent relative pressures), often leading to incomplete equilibration during uptake measurements in small-pore and medium-pore pore zeotypes [37].

Diffuse reflectance UV–visible spectra were used to probe the Ti species present in TS-1 and Au/TS-1 samples and to detect plasmon resonance bands that are characteristic of Au particles>2 nm in diameter. Spectra were acquired on powders (<100 μm diameter) using a Varian-Cary 6000i spectrometer and a Harrick scientific diffuse reflectance accessory (DRP-XXX) with a reaction chamber (DRA-2CR). Powders were held on a steel fritted disc that allowed uniform gas flow through the samples. A temperature controller (Watlow Series 982) connected to a heating element and a thermocouple (type K) embedded in the sample holder were used to maintain constant temperatures. The samples were treated within the cell in flowing He (1.67 cm^3 g^{-1} s^{-1}) at 623 K for 1 h in order to remove adsorbed water; the spectra were measured (200–800 nm) after cooling samples to ambient temperature in flowing He. Silicalite-1, synthesized as described in Section 2.2 but without the addition of Au, ligands, or Ti, or a white reflector ($BaSO_4$) were used to provide the background spectra required to convert reflectance data into pseudo-absorption intensities using the Kubelka-Munk formalism [38].

Infrared (IR) spectra were used to measure the extent of incorporation of Ti into the framework for TS-1 and Au/TS-1 samples; they were also used to determine the cleanliness of Au surfaces from the intensity and vibrational frequency of the infrared bands for chemisorbed CO. Transmission spectra were acquired using a Thermo Nicolet 8700 spectrometer on samples consisting of wafers (40 mg cm^{-2}) prepared from finely ground samples. The wafers were held in a controlled atmosphere cell equipped with CaF_2 windows, cartridge heaters, and liquid N_2 as a coolant. All samples were heated to 523 K at a rate of 0.033 K s^{-1} in flowing He (40 cm^3 g^{-1} s^{-1}) and held for 1 h; they were then cooled to 263 K or ambient temperature before spectra were acquired (400–2200 cm^{-1}). IR spectra at ambient temperature were used to examine vibrations resulting from the presence of framework Ti species and were conducted in a He atmosphere. IR spectra at sub-ambient temperatures were used to determine the cleanliness of Au nanoparticles from the intensity of the IR bands for CO chemisorbed on Au metal surfaces. In these experiments, samples were cooled to 263 K in He flow and then exposed to a 0.1–1.0% CO/He stream (40 cm^3 g^{-1} s^{-1}) for 0.25 h before collecting spectra. IR absorption features derived from CO(g) were subtracted from all collected spectra.

2.5. Catalytic assessment of reactivity and selectivity of confined Au nanoparticles in TS-1

2.5.1. Assessment of encapsulation selectivity of Au nanoparticles within TS-1 using large organosulfur molecules as titrants

The encapsulation selectivity of Au particles within TS-1 was determined by measuring ethanol (EtOH) oxidative dehydrogenation (ODH) turnover rates (per surface Au atom; Eq. (2)) on Au/TS-1 and Au/SiO_2 (prepared by deposition–precipitation, as described elsewhere [23]) before and after exposure to dibenzothiophene (DBT). DBT (0.9 nm kinetic diameter [39]) binds irreversibly to Au surfaces [23], but cannot diffuse through the small apertures in MFI (0.55 nm [40]) or other 10-MR zeotypes with similar frameworks, such as TS-1; it is thus prevented from contact with any Au nanoparticles located within TS-1 crystals. These titration procedures can be used to calculate the fraction of Au surface area in each sample that resides within the protected environment of TS-1 voids from the decrease in rate upon DBT titration for Au/TS-1 and Au/SiO_2 samples.

Au/TS-1 and Au/SiO_2 were exposed to DBT before rate measurements by agitating (with a magnetic bar at 6.7 Hz) an ethanol suspension of the powders at ambient temperature (300 cm^3 g^{-1}) that also contained DBT at a DBT:Au molar ratio of 6:1. Samples were exposed to the DBT solutions for a period of 4 h, a period that allows sufficient time for DBT to attach to accessible extracrystalline Au surfaces but not to substantially diffuse into 10-MR MFI apertures [23]. The treated samples were isolated by filtration, heated at 343 K for 12 h in a pre-heated convection oven containing ambient air, diluted ten-fold (by mass) with SiO_2, pelleted into 180–250 μm aggregates, and used in EtOH ODH reactions without further pretreatment (to minimize DBT desorption or decomposi-

tion). EtOH ODH rates were also measured on samples treated using identical protocols but without any DBT present in the contacting EtOH liquid media.

These catalyst aggregates were packed onto a porous quartz disk held within a quartz tube (10 mm OD) and heated to 393 K (at 0.017 K s^{-1}) using a resistively-heated tube furnace, a temperature controller (Watlow, 96 Series), and a type K thermocouple. The molar flow rates and composition of the inlet stream (9 kPa O_2, 4 kPa EtOH, 0.5 kPa H_2O, 87.5 kPa He) were metered using gas flow controllers (for He, O_2; Porter Instrument) or a liquid syringe pump (for H_2O, EtOH; Cole Parmer, 60,061 Series); all transfer lines before and after the reactor were kept above 343 K in order to vaporize EtOH and to prevent its condensation. The concentrations of EtOH and acetaldehyde (the only detected product) were measured using gas chromatography (Shimadzu GC-2014) with a methyl-phenyl-silicone capillary column (HP-5; 50 m × 0.32 mm, 1.05 μm film thickness) and a flame ionization detector. EtOH turnover rates are normalized here by the number of surface Au atoms present in each sample (estimated from their respective Au contents and TEM-derived size distributions; Eq. (2)). Reported EtOH turnover rates represent their values at <5% conversions during the initial stages of contacts with EtOH-O_2 co-reactants.

2.5.2. Assessment of Au/TS-1 reactivity and selectivity in propylene epoxidation using H_2O/O_2 reactants

Au/TS-1 samples (1.0% wt. nominal Au) with different mean Au nanoparticle sizes (3.8 ± 0.9 and 2.8 ± 0.5 nm; estimated by TEM, Section 3.2), prepared by post-synthetic thermal treatment (Section 2.3) in air alone (to give 3.8 nm Au particles with 0.9 nm standard deviation) or sequentially in He and air (2.8 ± 0.5 nm Au), were examined for use as propylene epoxidation catalysts using O_2/H_2O mixtures as co-reactants. Rates and selectivities to propylene oxide (PO) and other products (acrolein, propanal, isopropanol, CO_2) were measured on Au/TS-1 aggregates (180–250 μm) with and without mixing them physically with 180–250 μm quartz granules (1:1 by mass) in order to rule out any effects of bed temperature gradients caused by exothermic epoxidation reactions on measured rates. Reactions were examined on Au/TS-1 samples prepared both with and without the post-synthetic addition of alkali cations (Cs^+; Section 2.3), which have been suggested to be essential as enablers of propylene epoxidation reactivity with O_2/H_2O co-reactants on Au nanoparticles dispersed on TS-1 [11,12]. Elemental analysis using inductively-coupled plasma optical emission spectroscopy (ICP-OES) confirmed the absence of detectable K and Cs concentrations (<1 ppm) in all Au/TS-1 samples that were not deliberately post-synthetically doped with such species.

The apparatus, protocols, and molecular speciation methods used were the same as those described in Section 2.5.1, except for differences in the temperature (473 K), the inlet stream composition (3.7 kPa O_2, 3.7 kPa propylene; 6 kPa H_2O; 87.6 kPa He; 20,000–90,000 cm^3 $g_{cat}^{-1}h^{-1}$), and the capillary chromatographic column used (methyl silicone HP-1; 50 m × 0.32 mm, 1.05 μm film thickness). A packed column (Porapak-Q, 4.8 m, 80–100 mesh) connected to a thermal conductivity detector was used in parallel to detect and measure any CO or CO_2 molecules formed. Samples were heated in 20% O_2/He (1.67 cm^3 g^{-1} s^{-1}) to the reaction temperature (473 K) and then immediately exposed to the reactant gas mixture without any further pretreatment. Turnover rates are reported as the molar rate of PO formation per Au surface atom (estimated by TEM; Section 2.4); rates are also reported on a catalyst mass basis. All rates were measured at < 0.2% propylene conversion. No reactivity was detected on quartz granules or in empty reactors. All products formed (PO, acrolein, propanal, isopropanol) were identified from their elution times by the injection of certified pure standards using chromatographic protocols (Section S3, S4; SI) identical to those used for analysis of the reactor effluent.

3. Results and discussion

3.1. Effects of crystallization conditions on the stability of ligated Au precursors, solid product yield, and TS-1 phase purity

X-Ray diffractograms of as-synthesized TS-1 and Au/TS-1 (1% wt. nominal Au loading) crystallized using the IZA procedures (448 K; 48 h; Section 2.2; [29]) are shown in Fig. 1. Au/TS-1 gels held at 448 K for 48 h led to crystalline TS-1 (96% crystallinity, Section 2.4; Table 1), but also to the premature reduction and extensive agglomeration of Au-derived species into large Au metal crystallites (5–50 nm), as evident from transmission electron micrographs (Fig. 2). At these conditions (448 K; 48 h), the presence of Au^{3+} and MPS ligands within the synthesis gel did not substantially interfere with the assembly of titanosilicate oligomers as TS-1 crystallites, apparently because Au^{3+}-MPS coordination compounds are present as minority species (T-atom:MPS molar ratio of 48:1, where T = Si, Ti for MPS:Au molar ratio of 6:1 in this sample) and form large Au crystallites at extracrystalline locations where they cannot obstruct crystal growth. Au/TS-1 gels crystallized at slightly lower temperatures (438 K) for 48 h also showed sharp TS-1 diffraction lines (Fig. 1) and large Au nanoparticles (Fig. 2). Even lower temperatures (423 K, 48 h) also led to premature deprotection of ligated Au precursors (Fig. 2), but also to less crystalline solids than for TS-1 samples prepared using standard procedures (73%; Table 1) and to the formation of an amorphous phase (evident from a weak broad background in diffractograms; Fig. 1). The weak effects of Au^{3+} coordination complexes on the crystallinity of Au/TS-1 gels treated at 438–448 K suggest that the formation of amorphous phases in Au/TS-1 crystallized at 423 K largely reflects the lower synthesis temperature, which sought, but appears to have failed, to prevent the premature deprotection of Au^{3+} complexes. The high temperatures typically required to crystallize Ti-containing zeotypes (>443 K) reflect, in part, a proposed inhibitory effect of Ti precursors, even at very low Ti/Si ratios, on the rates of crystallization of silicate frameworks [41].

Au/TS-1 synthesis gels were crystallized at lower temperatures (393–413 K) for longer times (up to 120 h) than in previously reported syntheses (448 K; 48 h) in an attempt to: (i) prevent deprotection of ligated Au^{3+} precursors and (ii) compensate for the effects of low temperatures on TS-1 crystallinity through longer crystallization times. Fig. 3 shows the diffractograms of as-synthesized Au/TS-1 samples crystallized at 413 K for 48, 72, 96, and 120 h. The phase purity of TS-1 frameworks increased monotonically from 73% to 92% with longer synthesis times (48 h to 120 h); these trends confirm the intended compensation for lower temperatures by longer times in enabling crystallization. Hydrothermal synthesis of Au/TS-1, even at 413 K, however, led to the formation of large Au metal agglomerates, as evident from electron micrographs (Fig. 2; Table 1), indicating that Au complexes reduce and form Au^0 colloids at 413 K before these ligated precursors can be occluded within TS-1 crystals as they form.

Au/TS-1 samples prepared by hydrothermal crystallization at 393 K for 120 h, however, showed no detectable Au particles in micrographs (Fig. 2), suggesting that MPS ligands can protect Au^{3+} cations from reduction and precipitation at 393 K. The high crystallinity of this sample (93%; Table 1) also indicates that TS-1 frameworks can be formed at much lower temperatures than prescribed in accepted synthesis protocols (448 K). The solids yield for this Au/TS-1 sample was lower (65%; Table 1) than in the TS-1 sample prepared via standard procedures (448 K, 48 h), indicating

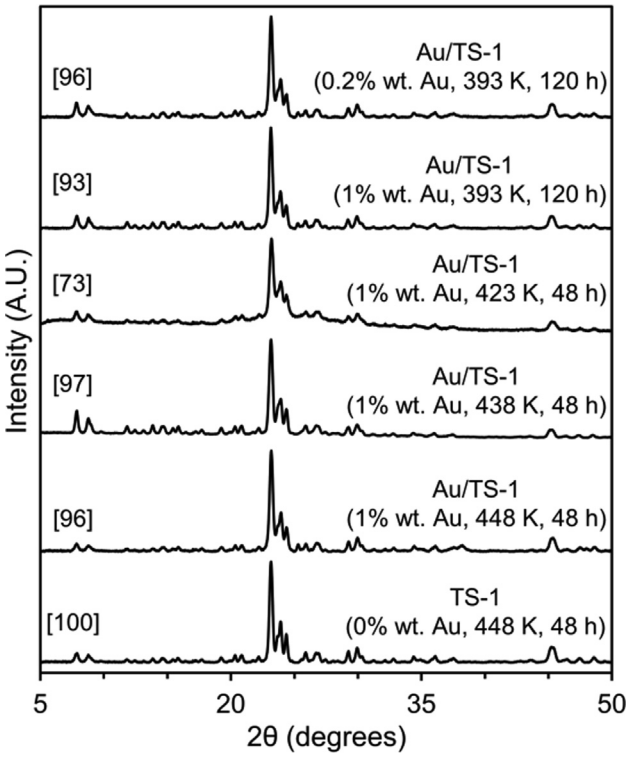

Fig. 1. X-Ray diffractograms of as-synthesized TS-1 crystallized at 448 K for 48 h, and Au/TS-1 (0.2–1% wt. nominal Au loading) crystallized at 448 K for 48 h, 438 K for 48 h, 423 K for 48 h, and 393 K for 120 h. The Au/TS-1 sample with 0.2% wt. Au loading was crystallized in the presence of 10% wt. TS-1 seed crystals. Framework crystallinities (%) relative to the TS-1 standard are shown in brackets.

that a larger fraction of the Si and Ti precursors were removed with the supernatant liquids during filtration (Section 2.2).

The addition of as-synthesized TS-1 seeds that were post-synthetically rinsed but not heated in air (10% wt. based on expected solid yields of TS-1 using standard synthesis protocols; Section 2.2; 48 h at 448 K) to Au/TS-1 synthesis gels before crystallization for 120 h at 393 K substantially increased solids yields (85%; Table 1), even after accounting for the contribution of the added seeds to the final product. Seed crystals may provide silicate and titanosilicate oligomers that promote crystal growth through their addition to growing proto-zeolitic moieties or via spalling of small nuclei during hydrothermal treatments to initiate crystal growth [42,43].

These synthesis procedures (Section 2.2) and crystallization conditions (393 K for 120 h with 10% wt. seeds) were also used to prepare an Au/TS-1 synthesis gel with 0.2% wt. nominal loading; this sample also showed TS-1 frameworks with high crystallinity (96%; Fig. 1) and yields (89%) without any microscopy evidence for large Au nanoparticles (Section S5, SI). The similar framework crystallinities and product yields for 0.2% wt. and 1.0% wt. Au/TS-1 samples (crystallinity: 96%, 94%; yield with 10% wt. seeds: 89%, 85%; for 0.2% and 1.0% wt. nominal Au loading, respectively) indicate that the crystallization conditions used for Au/TS-1 synthesis gels have a controlling effect on the assembly of TS-1 crystals over the range of metal contents examined. Such weak effects of the amount of metal–ligand complexes reflect their sparse presence within the TS-1 synthesis gels (T-atom:MPS molar ratios of 48:1 and 240:1; 0.27 and 0.06 metal complexes per unit cell for 1.0 and 0.2% wt. Au loading samples, respectively).

In the next section, X-ray diffraction, infrared spectroscopy, UV–visible spectroscopy, and electron microscopy data are shown for these samples after the post-synthetic oxidative and reductive treatments required to remove synthetic residues (Section 2.3) in order to assess the size and surface cleanliness of Au particles and the structural stability of the TS-1 crystals.

3.2. Characterization of Au/TS-1 samples after thermal treatments

The ultimate use of Au/TS-1 as a catalyst requires post-synthetic treatments that are able to remove bound ligands and occluded organic structure-directing agent (OSDA) species and to form small Au nanoparticles. The oxidative removal of OSDA compounds is exothermic and prone to cause high local temperatures that would promote Au particle growth [23]. Thermal treatment protocols that preserve small monodisperse Au particles, while fully removing synthetic residues, are therefore essential; they were developed as part of this study by assessing the effects of temperature ramping sequences and treatment gases on the size and surface cleanliness of Au nanoparticles. Such studies also examined the impact of such protocols on framework pore volumes, which provide a measure of the fraction of the solid that is present as crystalline zeotypes and of the accessibility of their void structures to reactant molecules.

Thermal treatments in air with intermediate holding periods at six different temperatures between 448 and 773 K (498, 548, 573, 623, 673, and 723 K; Section S1, SI) and a final hold at 773 K led in all cases to the formation of small (<5 nm) Au nanoparticles in Au/TS-1 (1.0% wt. nominal Au loading). The use of He (instead of air) during an initial period of sustained heating at 648 K, followed by subsequent treatment in air up to 773 K (Section S2, SI), led to smaller Au particles (2.8 nm) than those obtained after treatments in air alone. The stability conferred by the initial use of He appears to reflect the partial pyrolysis and removal of organic

Table 1
Crystallization temperature, crystallization time, presence of TS-1 seed crystals, stability of ligand-protected Au^{3+} cations, solid yields, and crystallinity of solid products for Au/TS-1 syntheses with 1% wt. nominal Au loading.

Crystallization Temperature (K)[a]	Crystallization Time (h)[b]	% Wt. Added Seed Crystals[c]	Au Precursor Stability[d]	% Solid Yield[e]	% Product Crystallinity[f]
448	48	0	Unstable	97	96
438	48	0	Unstable	98	97
423	48	0	Unstable	90	73
413	48	0	Unstable	44	73
413	120	0	Unstable	75	92
393	120	0	Stable	65	93
393	120	10	Stable	85	94

[a]Temperature of synthesis gel during hydrothermal assembly. [b]Duration of hydrothermal assembly. [c]Seed crystals consist of as-synthesized TS-1 crystallized at 448 K for 48 h; % wt. added seeds is based on the yield of TS-1 synthesized at 448 K for 48 h (5.48 g; Section 2.2). [d]The presence of Au agglomerates visible in electron micrographs of as-synthesized Au/TS-1 indicates that Au^{3+}-MPS precursors are unstable at the crystallization conditions. [e]Solid product yields are normalized by the yield of TS-1 synthesized at established conditions (448 K; 48 h; 5.48 g; Section 2.2) plus the additional weight of any added seed crystals. [f]Calculated from XRD using the integrated intensities of the three most intense diffraction lines, with TS-1 crystallized at 448 K for 48 h as a standard (Section 2.2).

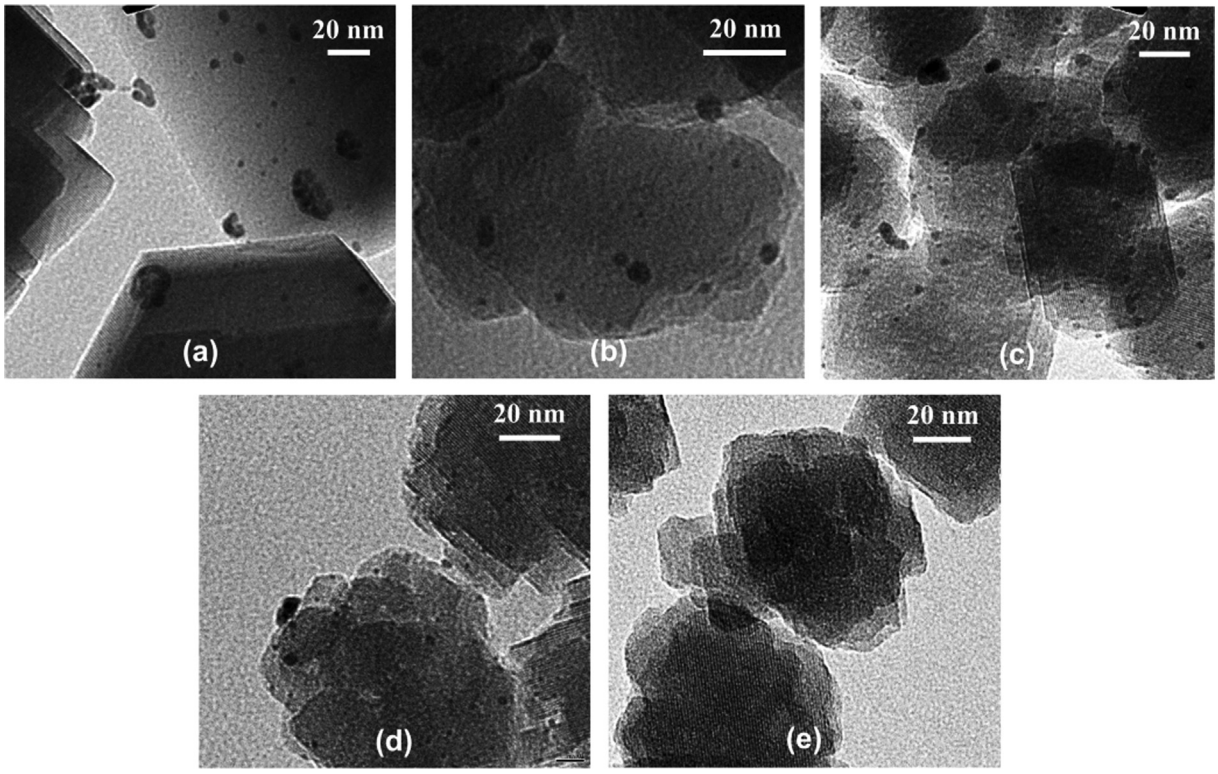

Fig. 2. Transmission electron micrographs of as-synthesized Au/TS-1 crystallized with 1% wt. nominal Au loading and without seed crystals at (a) 448 K for 48 h, (b) 438 K for 48 h, (c) 423 K for 48 h, (d) 413 K for 120 h, and (e) 393 K for 120 h.

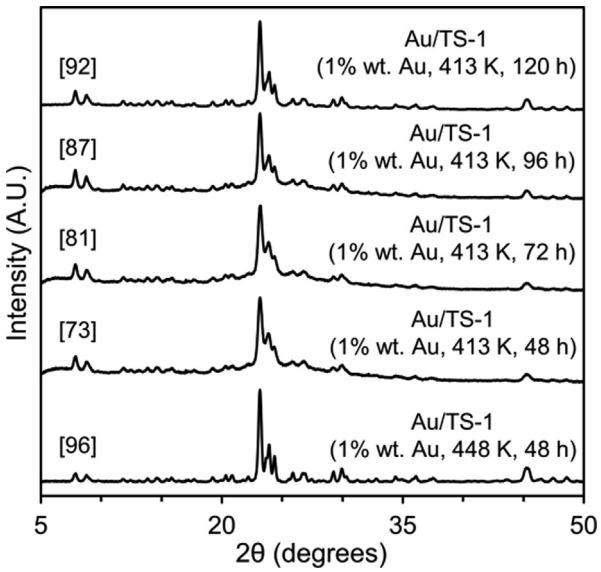

Fig. 3. X-Ray diffractograms of as-synthesized Au/TS-1 (1% wt. nominal Au loading) crystallized without seed crystals at 448 K for 48 h, and at 413 K for 48 h, 72 h, 96 h, and 120 h. TS-1 framework crystallinities (%) relative to an Au-free TS-1 standard are shown in brackets.

species in He, which moderates exotherms during subsequent oxidative treatments, thus preventing sintering of the Au nanoparticles. Direct heating to 773 K in air resulted in large (>5 nm) Au domains, a likely consequence of localized heating from the combustion of the organic templates. A final treatment in H_2 at 723 K led to higher CO chemisorption uptakes than air and He treatments alone, plausibly as a result of the removal of bound sulfur species derived from MPS ligands by H_2, but not by O_2 or inert gas. Detailed descriptions of the sequential pyrolytic, oxidative, and reductive treatments developed and used for Au/TS-1 (0.2–1.0% wt. nominal Au loading; crystallized with 10% wt. TS-1 seeds at 393 K for 120 h) are included in Section 2.3 and shown diagrammatically in Sections S1 and S2 (SI).

3.2.1. Framework crystallinity, micropore volume, and Au nanoparticle size after post-synthetic treatments of Au/TS-1

The diffractograms (Fig. 4) of Au/TS-1 samples prepared by staged thermal treatments in air alone (Section 2.3) show that TS-1 frameworks maintain the same crystallinity after post-synthetic treatments (96% and 93% for Au/TS-1 with 0.2% wt. and 1.0% wt. nominal Au loading, respectively) as before such treatments (96% and 94%). The Au contents in Au/TS-1 samples (0.2% wt. and 0.9% wt. Au; ICP-OES) are consistent with the nearly quantitative incorporation of all Au precursors present in gels within crystalline solids (0.2–1.1% wt. Au, respectively). These high Au uptake yields seem to reflect the preferential formation of siloxane linkages between the MPS ligands and protozeolitic precursors, which encourage the embedding of ligated precursors within zeotype crystals as the latter form [23,26]. Post-synthetic treatment of 0.9% wt. Au/TS-1 with air or by combined air and pyrolysis treatments led to the formation of relatively small Au particles ($\langle d_{TEM} \rangle$: 3.8 nm and 2.8 nm, respectively; Eq. (1); Fig. 5) uniformly distributed in size (DI: 1.11 and 1.10; Eq. (3)). Such particles are substantially larger than the largest voids present within TS-1 frameworks (channel intersections; 0.64 nm [40]). The evidence shown in Section 3.2.4 indicates that these Au nanoparticles are protected from contact with bulky organosulfur titrants, even though their size must have required local disruptions of the zeotype frameworks. The small size and selective intracrystalline confinement of these Au nanoparticles are consistent with the uniform distribution of ligated Au precursors throughout TS-1 crystals during the nucleation and growth of the crystalline framework. This,

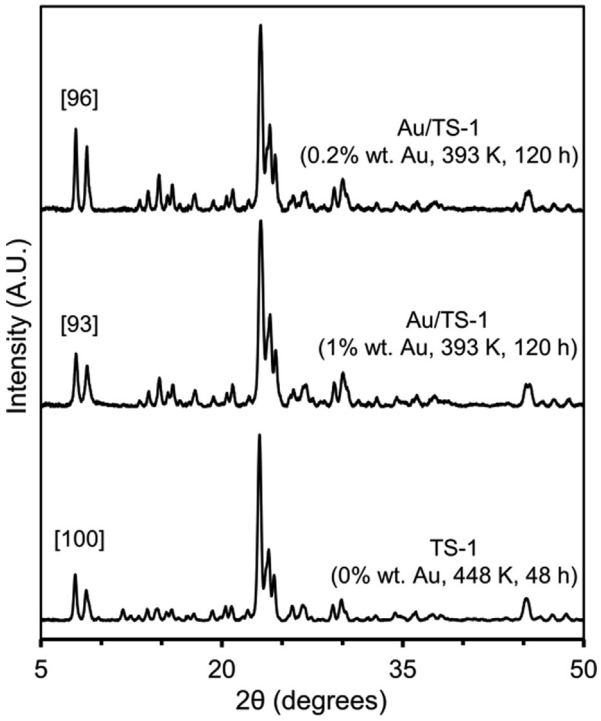

Fig. 4. X-Ray diffractograms of TS-1 crystallized at 448 K for 48 h and post-synthetically treated in flowing dry air (1.67 $cm^3\ g^{-1}\ s^{-1}$) at 823 K for 4 h, and Au/TS-1 crystallized at 393 K for 120 h in the presence of 10% wt. seed crystals with 0.2–1% wt. nominal Au loading, and post-synthetically treated in air and H_2 with staged thermal ramping procedures (Section 2.3). TS-1 framework crystallinities (%) relative to the TS-1 standard are shown in brackets.

combined with the energetic penalties imposed by the need to disrupt the confining crystalline framework in order to accommodate even larger Au particles, mitigate the growth of nanoparticles upon ligand removal [23,26] at conditions where unconfined nanoparticles become much larger [23–27]. Post-synthetic treatments of Au/TS-1 with lower Au contents (0.2% wt. Au, nominal and measured) led to Au nanoparticles ($\langle d_{TEM}\rangle$=3.6 nm; DI = 1.12) nearly identical in size and uniformity to those in the Au/TS-1 sample with 0.9% wt. measured Au loading ($\langle d_{TEM}\rangle$=3.8 nm; DI = 1.11).

These limiting nanoparticle sizes are essentially independent of Au content, an observation that appears to reflect the requirement for local disruptions of the TS-1 frameworks to accommodate further growth; this imposes a thermodynamic barrier to growth as particles reach a specific size for which their decrease in surface energy can no longer compensate for the energy required to locally disrupt the surrounding crystalline frameworks [23,24,26]. Such thermodynamic barriers also account for the thermal stability of Au nanoparticles in Au/TS-1, which are relatively small and monodisperse in size, in spite of the high temperature treatments in air (773 K) and H_2 (723 K) used in the post-synthetic treatment procedures (Section 2.3). The disruptions required to accommodate 2.8–3.8 nm Au particles within TS-1 voids (0.64 nm) do not measurably influence framework crystallinity (Fig. 4), because such Au nanoparticles occupy<0.3% of the microporous void volume of TS-1, even for the sample with the higher Au content (0.9% wt.).

The complete removal of the organic template and the ligands by these thermal treatments (Section 2.3) was confirmed from micropore volumes determined from CO_2 uptakes at 273 K (1–107 kPa; Section S6, SI) and from elemental sulfur analysis (ICP-OES). The CO_2-derived micropore volume of Au/TS-1 with 0.9% wt. Au (0.17 $cm^3\ g^{-1}$; Section S6, SI) matched that of the metal-free TS-1 standard treated in air at 823 K for 4 h (0.16 $cm^3\ g^{-1}$; Section S6, SI) and that of a silicalite-1 standard (0.20 $cm^3\ g^{-1}$; [37]). The ligands added to the TS-1 synthesis gels could occupy, at most, 0.08 $cm^3\ g^{-1}$ of micropore volume in the crystallized Au/TS-1 (1.0% wt. nominal Au loading), even if post-synthetic treatments were completely ineffective at removing such ligands. The sulfur content was not detectable by ICP-OES (<1 ppm) in Au/TS-1 with 0.9 wt% Au after post-synthetic sequential treatments in air and then H_2 (Section S1, SI), indicative of the full removal of at least the S-moiety in these ligands.

3.2.2. Assessment of Au surface cleanliness and accessibility using infrared spectra of chemisorbed CO

Infrared spectra of chemisorbed CO were used to confirm the absence of S-containing ligands and the cleanliness and accessibility of exposed Au nanoparticle surfaces. CO was used as the titrant of Au surface atoms, instead of O_2 or H_2, because the latter dissociate very slowly at the low temperatures required to achieve detectable coverages [44] and neither one provides a spectroscopic signature that reflects the binding properties of Au nanoparticle surfaces.

Fig. 6 shows infrared spectra for chemisorbed CO (at 263 K, 1 kPa CO) on Au/TS-1 ($\langle d_{TEM}\rangle$=3.8 nm; 0.9% wt. Au; DI 1.11) and Au/SiO_2 ($\langle d_{TEM}\rangle$=2.7 nm; 2.2% wt.; DI 1.06; prepared by deposition–precipitation). CO infrared band intensities were

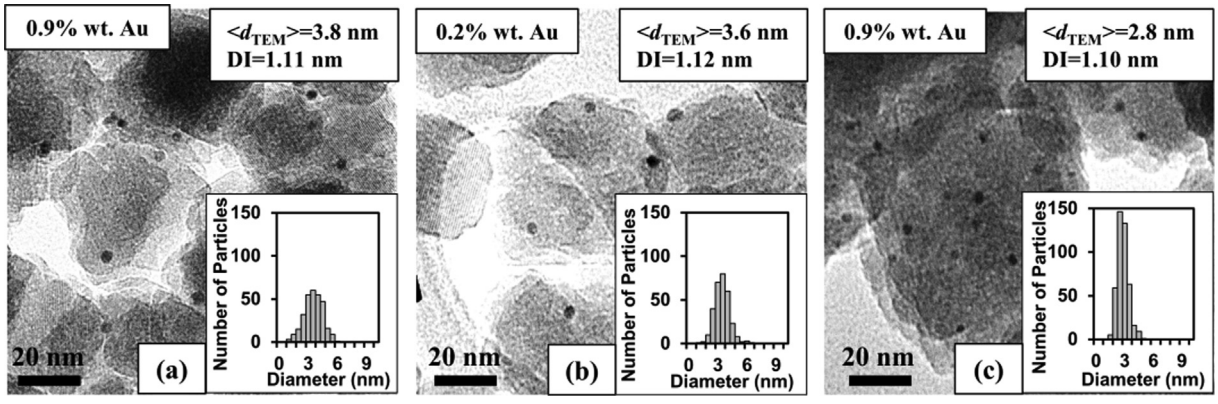

Fig. 5. Transmission electron micrographs, surface-averaged nanoparticle diameters ($\langle d_{TEM}\rangle$, Eq. (1)), particle dispersity indexes (DI, Eq. (3)), and nanoparticle diameter distributions for post-synthetically treated Au/TS-1 (0.2–1.0% wt. nominal Au loading) crystallized at 393 K for 120 h with 10% wt. seed crystals. Micrographs in (a) and (b) corresponds to Au/TS-1 treated via staged thermal ramping first in air alone and then in H_2; the sample in micrograph (c) was treated via staged thermal ramping first in He, followed by air, and then in H_2 (Section 2.3).

normalized by the number of surface Au atoms in each sample, estimated from measured Au metal loadings and nanoparticle dispersion values (Eq. (2)). Previous studies have shown that the deposition–precipitation method used to prepare Au/SiO_2 forms Au surfaces devoid of any synthetic debris and that Au surfaces bind CO at near saturation coverages at the conditions used to obtain these infrared spectra (263 K, 1 kPa CO; [23]).

Au/TS-1 and Au/SiO_2 show infrared absorption bands (at ~2110 cm^{-1}) corresponding to the carbonyl stretch in CO bound on Au^0 surfaces [45]. The ratio of accessible Au atoms in these two samples (Ω) is defined as:

$$\Omega = \frac{\tilde{I}_{Au/TS-1}}{\tilde{I}_{Au/SiO_2}} \quad (4)$$

where $\tilde{I}_{Au/TS-1}$ and $\tilde{I}_{Au/SiO_2}$ are the integrated Au-CO band intensities (normalized by the number of surface Au atoms) for Au/TS-1 and Au/SiO_2, respectively, at each CO pressure. The $\tilde{I}_{Au/SiO_2}$ value is used as a reference because Au surfaces in Au/SiO_2 are known to be accessible and free of contaminants [23]. A Ω value of about unity would indicate that Au surfaces in Au/TS-1 are also accessible and free of any synthetic debris derived from MPS ligands or OSDA species. The calculated values of Ω (0.84–0.97) are near unity at all pressures (0.1–1.0 kPa CO), indicating that the post-synthetic thermal treatments used here for Au/TS-1 samples (Section 2.3) are able to remove essentially all organic and sulfur species from Au nanoparticle surfaces. The Au nanoparticles in Au/TS-1 shown in electron micrographs (Fig. 5) are therefore accessible and free of surface contaminants.

3.2.3. Characterization of Ti species using infrared and UV–visible spectra

Highly dispersed and tetrahedrally coordinated Ti atoms in TS-1 frameworks are the most active structures for alkene epoxidation [8,11,12]. The predominant presence of Ti species as tetrahedrally-coordinated atoms within the silicate framework of the Au/TS-1 samples prepared by the methods reported here would indicate that these synthetic and post-synthetic treatment procedures (Section 2.2-2.3) did not adversely influence the extent of Ti incorporation [29]. Ti species within the silicate framework exhibit spectral features that are distinct from those in extra-framework Ti structures in the infrared and UV–visible spectral range.

The predominant presence of tetrahedrally-coordinated Ti centers within TS-1 frameworks was confirmed from framework vibrations at 960 cm^{-1} and 800 cm^{-1} in their infrared spectra [46]. The band at 960 cm^{-1} corresponds to Si-O vibrations associated with Si atoms near framework Ti [46]; it is the accepted metric of the extent of incorporation of Ti atoms into silicate frameworks. The intensity of this band relative to the reference absorption band at 800 cm^{-1} (characteristic of pentasil frameworks [46]) reflects the amount of Ti present within the silicate framework in TS-1. The ratios of intensities for the 960 cm^{-1} and 800 cm^{-1} bands in the standard TS-1 sample (crystallized at 448 K for 48 h; Si/Ti = 78, measured by ICP-OES) and in the Au/TS-1 samples crystallized at 393 K (for 0.2% wt. Au sample: Si/Ti = 74; 0.9% wt. Au sample: Si/Ti = 76) are expected to be similar if the extent of Ti incorporation in Au/TS-1 is unaffected by its lower synthesis temperature (393 K vs. 448 K) or by the presence of seed crystals or ligated Au^{3+} during synthesis (Section 2.2).

The infrared spectra of the TS-1 standard and of two Au/TS-1 samples are shown in Fig. 7. The ratio of the absorption bands at 960 cm^{-1} and 800 cm^{-1} was similar for TS-1 (1.17) and Au/TS-1 (1.08 and 1.06 for 0.2% wt. and 0.9% wt. Au samples, respectively), consistent with the predominant presence of Ti atoms within the silicate framework in all samples. These intensity ratios (TS-1: 1.17; Au/TS-1: 1.06–1.08) are those expected based on previous reports for TS-1 frameworks with slightly higher Ti contents (absorption band ratio of 1.50 for Si/Ti ratio of 53.5) [46].

UV–visible spectra were collected for TS-1 and Au/TS-1 samples after post-synthetic oxidative and reductive treatments (Section 2.3) in order to probe the coordination environment of Ti species. TS-1 and Au/TS-1 samples were treated in He (1.67 $cm^3\ g^{-1}\ s^{-1}$) at 623 K for 1 h within the diffuse reflectance UV–visible cell before acquiring spectra at ambient temperature in flowing He (Section 2.4). These treatments sought to remove bound water, which interacts with tetrahedrally-coordinated (framework) Ti centers to form complexes with spectral features in the same wavelength range (250–300 nm; [7]) as extra-framework Ti oxides (~270 nm; [47]). H_2O_2 or hydroperoxy species can form on Au surfaces in the presence of H_2O and O_2 [10] and can also interact with nearby framework Ti sites to form Ti-OOH complexes that give a broad absorption band in a wavelength range (~340 nm; [7]) where anatase TiO_2 also absorbs (320 nm; [47]). Such extraneous effects thus require the removal of water for unambiguous interpretations of the UV–vis spectra for TS-1 and Au/TS-1; these spectra are shown in Fig. 8 after subjecting samples to these dehydration protocols.

The spectra of the TS-1 standard and the Au/TS-1 (0.2% wt. Au) sample were corrected by subtracting the silicalite-1 spectrum (SIL-1 is the same crystal structure as TS-1 but without any Ti atoms). Both samples show a sharp absorption band at 220–230 nm after background subtraction. This absorption feature corresponds to tetrahedral Ti centers within the silicate framework [15]. The spectra do not exhibit detectable features in the 270–330 nm range, which are typically attributed to extra-framework Ti species [18,47]. The spectrum for Au/TS-1 with 0.2% wt. Au showed an additional absorption feature of moderate intensity at about 520 nm, corresponding to the surface plasmon resonance feature for Au nanoparticles [48]. The spectrum of the Au/TS-1 sample with higher Au content (0.9% wt. Au; with silicalite-1 or $BaSO_4$ as the subtracted background) is dominated by an intense plasmon absorption band at ~520 nm and an accompanying broad background absorbance between 250 and 600 nm, which would interfere with any of the bands for Ti species in the relevant wavelength range (220–330 nm). The prominence of these absorbance features reflects significant plasmon-induced enhancements of the extinction coefficients for nearby Si and Ti species [49]. The absorption bands for Ti species in 0.9% wt. Au/TS-1 were extracted from their spectrum by subtracting the spectrum for Au/silicalite-1 with similar Au content, synthesized and post-synthetically treated using identical procedures (but without the presence of the Ti precursors; Section 2.2). Such a reference spectra accounts for most of the features in Au/TS-1; the difference spectrum clearly shows the absorption feature at 220–230 nm, which corresponds to tetrahedral framework Ti centers (Fig. 8).

The Au/TS-1 samples with 0.2% and 0.9% wt. Au contents (but not the Au-free TS-1 sample) showed a weak absorption feature near 270 nm, indicative of traces of extra-framework Ti [47]. Such species may consist of Ti defect sites within the TS-1 framework, possibly arising from interruptions in the framework periodicity imposed by the attachment of MPS ligands to nucleating titanosilicates; they could also result from the disruptions of the void structure required to confine any Au nanoparticles that are larger than the TS-1 intersections or channels. The concentration of these defects or extra-framework Ti species, however, is very small compared to tetrahedrally-coordinated Ti incorporated into TS-1, as indicated by the relative magnitude of the bands at about 225 and 270 nm and confirmed by independent evidence from the infrared data (Fig. 7).

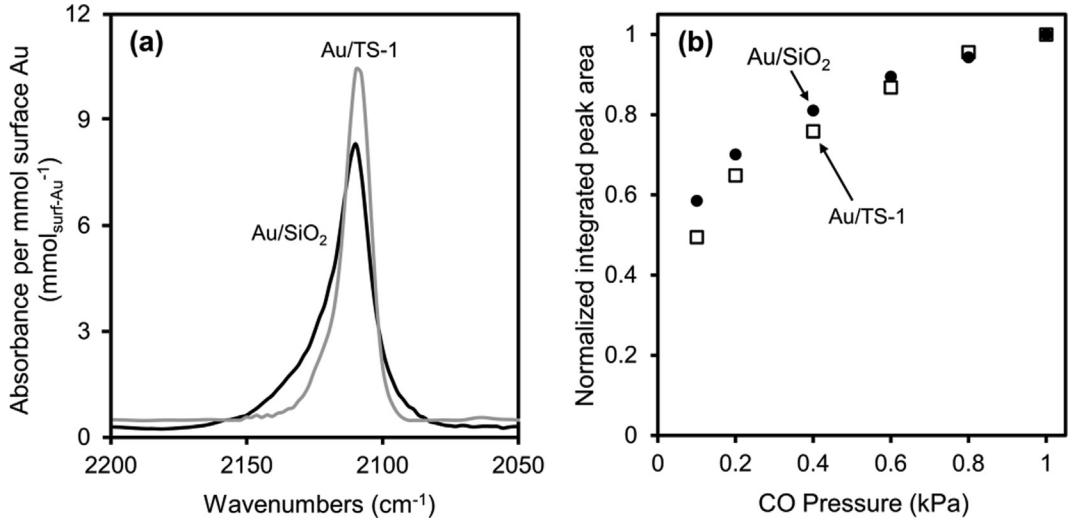

Fig. 6. (a) Infrared spectra of CO adsorbed on Au nanoparticles in Au/SiO_2 (black) and Au/TS-1 (0.9% wt. Au, gray) samples at 263 K (1.0 kPa CO, 99.0 kPa He) after flowing He pretreatment (473 K, 1 h). Intensities are normalized by the moles of surface Au atoms in each sample, estimated from TEM-derived particle sizes (Eq. (1)) and Au particle dispersions (Eq. (2)). (b) Integrated absorption band area of Au/SiO_2 (●) and Au/TS-1 (0.9% wt. Au, □) at 0.1–1.0 kPa CO and 263 K. Absorption band areas are normalized by the maximum area (collected at 1.0 kPa CO) for each sample.

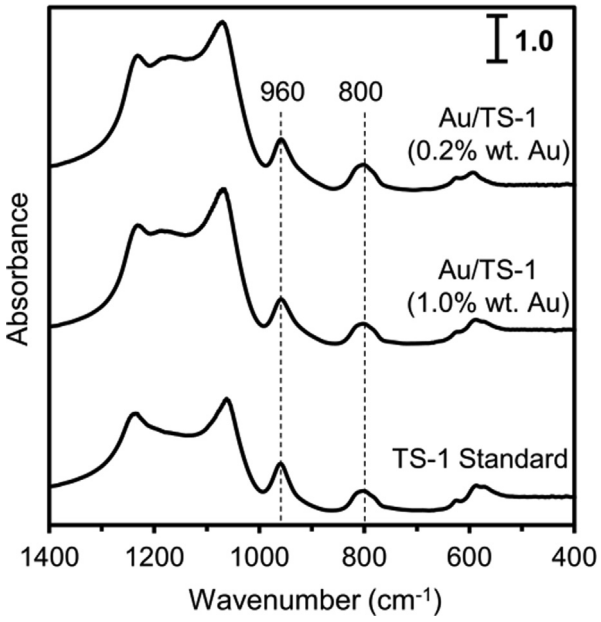

Fig. 7. IR spectra of post-synthetically treated (Section 2.3) TS-1 and Au/TS-1 (with 1.0% wt. and 0.2% wt. nominal Au loading) in a He atmosphere at ambient temperature.

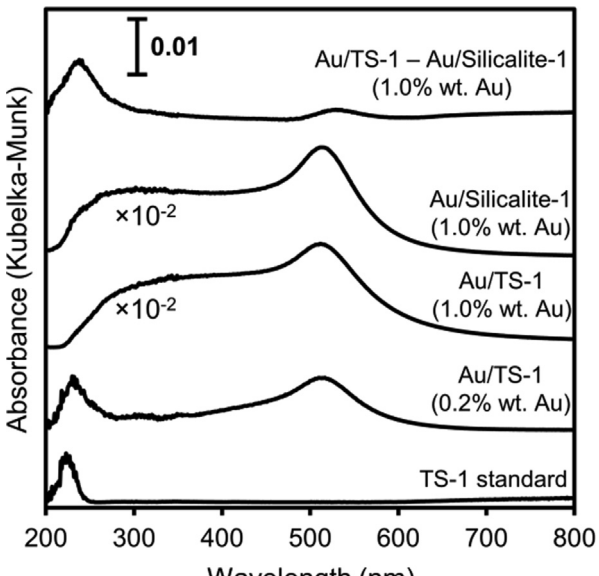

Fig. 8. UV–vis spectra of post-synthetically treated TS-1, Au/TS-1 (with 0.2% wt. and 1.0% wt. nominal Au loading), and Au/silicalite-1 (1.0% wt. nominal Au loading) in a He atmosphere at ambient temperature. Also shown is the difference spectra resulting from the background correction of the absorbance spectrum of Au/TS-1 with the spectrum of Au/silicalite-1 (both with 1.0% wt. nominal Au loading). $BaSO_4$ is the reference spectrum used for Au/TS-1 and Au/Silicalite-1 with 1.0% wt. nominal Au loading. The spectra of TS-1 and Au/TS-1 with 0.2% wt. nominal Au loading were background corrected using silicalite-1. Samples were treated in He (1.67 $cm^3\ g^{-1}\ s^{-1}$) at 623 K for 1 h prior to spectral acquisition.

3.2.4. Au encapsulation selectivities measured from dibenzothiophene titration effects on ethanol oxidation rates

Metal nanoparticles confined within microporous zeotypes are protected from contact with reactants or titrants that cannot diffuse through the apertures created by their crystalline frameworks [22–27]. Such sieving effects depend sensitively on the size and shape of the apertures and the molecules [22–27]; they are used here to determine the extent to which exposed surfaces of Au nanoparticles reside within the protective void structure of TS-1 crystallites.

Oxidative dehydrogenation (ODH) rates of ethanol (EtOH; 0.40 nm kinetic diameter [23]) were measured on Au/TS-1 and Au/SiO_2 catalysts before and after contacting these samples with a bulky organosulfur molecule (dibenzothiophene; DBT; 0.9 nm kinetic diameter [39]). DBT strongly binds onto any Au surfaces that it is able to contact [23], in this case any Au nanoparticles supported on mesoporous SiO_2 or present at external TS-1 crystal surfaces; such bulky titrants cannot reach Au surfaces protected by the small apertures in TS-1 frameworks (0.55 nm [40]). Consequently, ethanol ODH rates represent accurate reporters of the extent to which Au surfaces reside within TS-1 voids, because such surfaces would remain active even after samples are exposed to the bulky DBT titrants.

EtOH ODH rates (Section 2.5.1) were measured on DBT-treated samples ($r_{ODH,DBT}$) and on control samples (r_{ODH}). These rates were used to calculate an inhibition factor ($\lambda_{DBT,i}$), defined as:

$$\lambda_{DBT,i} = \frac{r_{ODH,DBT}}{r_{ODH}} \quad (5)$$

The value $\lambda_{DBT,Au/SiO2}$ reflects the residual EtOH turnover rates (expressed as a fraction) on Au/SiO_2 after DBT titration. A fraction of DBT-accessible Au surfaces in Au/SiO_2 and Au/TS-1 can retain some low rates after DBT treatment because these bulky DBT titrants may leave interstices accessible to EtOH and dioxygen [23]. As a result, the value of $\lambda_{DBT,Au/TS-1}$ does not directly reflect the fraction of encapsulated Au surfaces, because extracrystalline Au nanoparticles in Au/TS-1 would also retain some ODH activity even after DBT exposure. The encapsulation selectivity of Au nanoparticles within Au/TS-1 (F) is given by:

$$F = \lambda_{DBT,Au/TS-1} - \lambda_{DBT,Au/SiO2}\frac{(1-\lambda_{DBT,Au/TS-1})}{(1-\lambda_{DBT,Au/SiO2})} \quad (6)$$

The second term in Equation (6) rigorously corrects for residual EtOH ODH rates on titrated extracrystalline Au surfaces. EtOH ODH rates (r_{ODH}), inhibition factors (λ), and the Au encapsulation selectivity (F) for Au/TS-1 (0.9% wt. Au; $\langle d_{TEM}\rangle$=3.8 nm) are shown in Table 2.

The measured encapsulation selectivity for Au/TS-1 with 0.9% wt. Au (0.96; Table 2) confirms that most of the Au nanoparticles in this sample reside within the protected confines of TS-1 crystals. The values of $\lambda_{DBT,Au/TS-1}$ and F (0.96) were identical because of the negligible impact of correcting for inhibition factors using Equation (6), a reflection of the small contributions from the residual reactivity of unprotected Au surfaces after titration with DBT. EtOH ODH rates on untitrated Au/TS-1 (10×10^{-3} s^{-1}) were slightly lower than on Au/SiO_2 (12×10^{-3} s^{-1}), a likely consequence of intracrystalline EtOH concentration gradients within TS-1 crystals. Such diffusional constraints cause Equation (6) to underestimate the actual encapsulation selectivity, because of a concomitant underestimation of the true kinetic reactivity of intracrystalline Au surfaces.

These data, taken together with XRD, TEM, micropore volume, and spectroscopic characterization data (Sections 3.2.1-3.2.3), indicate that the synthetic strategies described in Section 3.1 indeed formed stable and clean Au nanoparticles that reside within TS-1 crystallites. TEM (Fig. 5) and infrared (Fig. 6) evidence show that Au nanoparticles are small, uniformly dispersed, and free of synthetic debris after the post-synthetic treatments developed in this study. Such nanoparticles are larger (2.8–3.8 nm) than the TS-1 channel intersections (0.55 nm [40]); yet, they reside predominantly (>96% of their exposed surfaces) within regions protected by the channels within these zeotype frameworks from contact with bulky organosulfur poisons. The low synthesis temperatures (393 K), long crystallization times (120 h), and the use of seed crystals (10% wt.), required to assemble Au/TS-1 without decomposing Au-MPS precursors, did not adversely affect framework crystallinity (Fig. 4; XRD), micropore volume (Section S6, SI), or Ti incorporation into the framework (IR, Fig. 7), which were essentially the same as on samples crystallized at the standard conditions of previous work (448 K; 48 h).

The potential of these Au/TS-1 systems for use as epoxidation catalysts provided much of the impetus for developing novel techniques to synthesize them, but the synthetic strategies developed are broadly applicable well beyond this specific application and original intent. In the next section, we present evidence for the propylene epoxidation reactivity of these samples using H_2O-O_2 reactants.

Table 2
Ethanol ODH turnover rates, inhibition factors, and encapsulation selectivities of Au/TS-1 and Au/SiO_2 samples.

Sample	r_{ODH} (10^{-3} s^{-1} $mol^{-1}_{surf\text{-}Au}$) [a]	Inhibition Factor (λ)[b]	Encapsulation Selectivity (F)[c]
Au/TS-1	10	0.96	0.96
Au/SiO_2	12	0.11	0[d]

[a] EtOH ODH turnover rates of samples agitated in liquid EtOH (300 cm^3 g^{-1}) at ambient temperature for 4 h and then used in reaction (9 kPa O_2, 4 kPa EtOH, and 0.5 kPa H_2O) at 393 K. Turnover rates are defined as the moles of EtOH converted per unit time normalized by the number of exposed metal surface atoms estimated from particle dispersions (Eq. (2)).
[b] $r_{ODH,DBT}/r_{ODH}$ (Eq. (5)), where $r_{ODH,DBT}$ are EtOH ODH rates measured on samples treated similarly but with DBT dissolved in the EtOH to achieve a 6:1 M ratio of DBT to Au.
[c] Encapsulation selectivity, defined as the fraction of active Au surface area encapsulated within zeotype crystallites, as estimated from λ values (Eq. (6)).
[d] Au surfaces fully accessible to DBT titrants.

3.3. Propylene epoxidation rates and selectivities on Au/TS-1 catalysts

Propylene epoxidation reactions are catalyzed by Au/Ti-oxide catalysts using either H_2/O_2 or H_2O/O_2 co-reactants, plausibly via the in-situ formation of highly-reactive HOOH or OOH intermediates on small Au nanoparticles; these molecular sources of electrophilic O-atoms then reach, through migration or atomic contact, Ti centers where epoxidation events occur [7,8,10]. H_2O/O_2 reactants give propylene oxide (PO) formation rates about ten-fold lower than H_2/O_2 mixtures [9,10,11], but fast parasitic reactions consume H_2 to form H_2O, often with high selectivity [14,20], thus making H_2O/O_2 mixtures a potential alternative, in spite of their lower reaction rates. Au nanoparticles confined within the microporous regions of TS-1 reside, on average, much closer to Ti centers than when deposited at extracrystalline surfaces or dispersed on mesoporous structures. The premise that HOOH (with H_2/O_2 reactants) or surface-bound *OOH (with H_2O/O_2) species must migrate to Ti centers within TS-1 before their intervening decomposition [10] would then lead to the expectation of kinetic benefits from such shorter Ti-Au distances or from more frequent atomic contact prevalent in encapsulated Au/TS-1 catalysts prepared by the methods reported here.

Au/TS-1 catalysts used previously for propylene epoxidation with H_2O/O_2 co-reactants contain Au nanoparticles (1.8–4.1 nm) deposited at very low loadings (0.19–0.34% wt. Au) at external TS-1 surfaces (Si/Ti = 50–105); they also contain K^+, Rb^+, or Cs^+ cations (1.0–3.0% wt. alkali cation) and their charge-balancing anions (CO_3^{2-}, OH^-, PO_4^{3-}) [11,12,50]. Alkali cations in atomic contact with Au nanoparticles were proposed to be required to stabilize the O_2^- species that react with H^+ species formed via heterolytic H_2O activation to form *OOH intermediates [11,12,50]. These cations are thought to enhance PO selectivities by titrating Ti-OH species that can act as Brønsted acid sites at external TS-1 crystal surfaces; such acid sites can catalyze PO isomerization to propanal via hydrolysis-dehydration-keto/enol isomerization sequences [11]. O* species formed via *OOH decomposition on Au surfaces may insert into the allylic C-H bond in propylene to form an enol, which in turn dehydrogenates to form acrolein as the predominant side product [11].

Propylene epoxidation rates and selectivities were measured (at 473 K, 3.7 kPa O_2, 3.7 kPa propylene, 6 kPa H_2O, 87.6 kPa He; Section 2.5.2) on Au/TS-1 catalysts prepared by the methods reported above ($\langle d_{TEM}\rangle$: 2.8 or 3.8 nm mean Au nanoparticle diameter; DI: 1.10 or 1.11; 0.9% wt. measured Au loading; Section 2.2-2.3) without any purposeful addition of alkali cations. These Au/TS-1 samples formed propylene oxide and other products, even though indigenous alkali species were not detectable (<1 ppm K or Cs;

ICP-OES). Selectivities to PO and byproducts at different bed residence times (2–9 × 10^4 cm^3 $g_{cat}^{-1}h^{-1}$) were used to assess their respective formation via primary or secondary events. The selectivities to the predominant products (>5.0% selectivity; C-basis), consisting of acrolein, PO, and propanal, are shown in Fig. 9. Isopropanol was also formed as a minor product (<5.0% selectivity at all residence times).

The selectivities determined by extrapolation to zero residence time (and propylene conversion) represent the relative rates of formation of each product in primary reaction events; the selectivity trends with increasing residence time reflect, in turn, the extent to which primary products react via subsequent events and what products they form. PO and acrolein form as primary products (initial selectivities 44% and 56%, respectively); propanal becomes detectable only as conversion increases and secondary reactions occur with increasing residence time. Acrolein and propanal selectivities increase monotonically with increasing bed residence time, while PO selectivity decreases, consistent with the secondary conversion of PO to propanal and/or acrolein; acrolein, but not propanal, also forms via primary reactions of propyelene-O_2-H_2O mixtures. These data indicate that all propanal molecules are derived from an initial turnover that formed PO. As a result, propylene epoxidation (PO formation) turnover rates are reported here as the combined rates of formation of PO and propanal; they are used along with acrolein formation rates to determine the intrinsic selectivity to these two primary products.

Fig. 10 shows PO and acrolein formation rates (per surface Au atom, Au dispersion values from Eq. (2)) and propylene conversion on Au/TS-1 catalysts ($\langle d_{TEM}\rangle$: 2.8 or 3.8 nm mean Au nanoparticle diameters; 0.9% wt. Au) at 473 K. Rates and selectivities remained essentially constant during the course of these experiments (average 6 h; up to 12 h).

PO and acrolein turnover rates (per exposed Au atom, based on TEM-detectable nanoparticles) on the Au/TS-1 sample with the larger nanoparticles ($\langle d_{TEM}\rangle$: 3.8 nm; r_{PO}: 5.2 × 10^{-5} s^{-1}; $r_{acrolein}$: 4.5 × 10^{-5} s^{-1}) are about ten-fold lower than those on Au/TS-1 with smaller Au domains ($\langle d_{TEM}\rangle$: 2.8 nm; r_{PO}: 63 × 10^{-5} s^{-1}; $r_{acrolein}$: 150 × 10^{-5} s^{-1}); these data indicate that smaller Au domains show much higher reactivity in forming the kinetically-relevant intermediates required for bifunctional epoxidation routes. These strong consequences of Au dispersion may reflect the higher reactivity of small Au nanoparticles for the formation of *OOH species that act as intermediates for PO and acrolein formation [11] or a larger number of Au nanoparticles on the more highly dispersed sample and the concomitant shorter distance between the Au and Ti functions. Disparities in activity between relatively small and large Au particles likely arise from the greater prevalence of highly coordinatively unsaturated surface Au atoms on the former.

The Au/TS-1 sample with larger Au domains gave a higher PO selectivity ($r_{PO}/r_{acrolein}$ = 1.2 vs. 0.41), suggesting an even stronger Au particle size effect on the formation rate of acrolein than PO. Propanal (22% selectivity on $\langle d_{TEM}\rangle$=3.8 nm and 16% on $\langle d_{TEM}\rangle$=2.8 nm) and isopropanol (4.0% and 0.2% selectivity, respectively) were also formed on both samples, but neither CO nor CO_2 were detected in any instance (<0.01%). Isopropanol is likely to form via propylene hydration on minority SiOH or TiOH acid centers. Propanal, by contrast, is produced in substantial quantities and likely forms as a secondary reaction product from PO on Brønsted acid sites [50]. A summary of these proposed reaction pathways is shown in Scheme 1.

The finding that PO forms on Au/TS-1 samples that lack detectable alkali species stands in contrast with the proposed requirement for alkali species to form *OOH intermediates from O_2-H_2O co-reactants [11,12,50]. PO turnover rates on the Au/TS-1 samples of the present study are significantly lower, however, than those reported on Cs-containing Au/TS-1 catalysts predominantly containing extra-crystalline Au clusters (0.20% wt. Au; Cs/Au = 15; 53.6% PO; 473 K; 10 kPa O_2; 10 kPa C_3H_6; 2.5 kPa H_2O; 0.22% conversion [11]), when compared on a per surface Au atom basis (5 × 10^{-5} to 63 × 10^{-5} s^{-1} vs. 660 × 10^{-5} s^{-1}). PO formation rates based on catalyst mass, however, are similar on the alkali-free Au/TS-1 samples of this study (0.08–1.3 × 10^{-8} mol_{PO} g_{cat}^{-1} s^{-1}) to

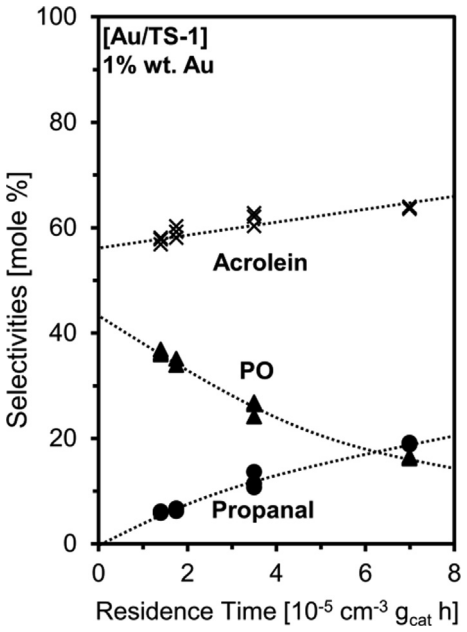

Fig. 9. Effect of bed residence time on acrolein, propanal and PO selectivities on Au/TS-1 (0.9% wt. Au; $\langle d_{TEM}\rangle$=3.8) at different bed residence times (473 K, 3.7 kPa propylene, 3.7 kPa O_2, 6.0 kPa H_2O). Curves are intended to indicate trends.

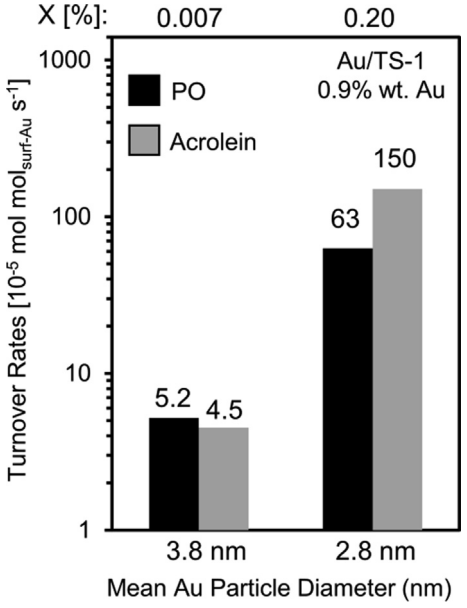

Fig. 10. Primary formation rates of PO (black) and acrolein (gray) on Au/TS-1 (0.9% wt. Au) post-synthetically treated in air alone (left) and sequentially in He and air (right) (Section 2.3). Rates are normalized by the number of Au surface atoms in each sample, estimated from Au nanoparticle dispersions (Eq. (2)) (473 K, 3.7 kPa propylene, 3.7 kPa O_2, 6.0 kPa H_2O, and 87.6 kPa He (60,000 cm^3 $g_{cat}^{-1}h^{-1}$). Propylene conversion (X, %) is listed at the top of the graph. The mean surface-averaged Au particle diameter (Eq. (1)) of each sample is given below respective data. Rates are reported after 2 h on stream, but remained essentially unchanged through the course of the experiments (average 6 h; up to 12 h).

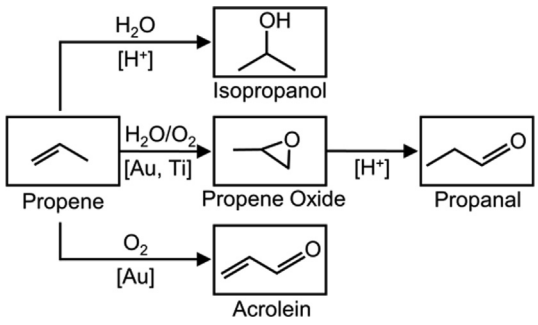

Scheme 1. Proposed reaction pathways for the formation of propene oxide and byproducts during propene epoxidation with H_2O/O_2 on Au/TS-1 catalysts lacking alkali promoters.

those reported on Cs-containing Au/TS-1 (1.89×10^{-8} mol_{PO} g_{cat}^{-1} s^{-1}). The mean diameter of the Au nanoparticles detected by TEM are similar for the Au/TS-1 prepared by the methods described here (2.8–3.8 nm) and in the aforementioned previous work (4.1 nm; [11]), suggesting that the observed differences in turnover rates do not reflect different Au particle diameters (at least for TEM-detectable nanoparticles).

Au/TS-1 samples prepared by the alkali-free methods reported here were impregnated with aqueous Cs_2CO_3 solutions (Section 2.3) to determine any influence of alkali on epoxidation rates with H_2O/O_2 reactants. The addition of Cs (0.9% wt. Au; $\langle d_{TEM} \rangle$: 3.8 nm; Cs/Au at. = 7–12) led to the exclusive formation of PO and acrolein as detectable products on such alkali-promoted Au/TS-1 samples at rates reported in Table 3. The presence of Cs specifically suppressed the formation of isopropanol and propanal, consistent with the titration of protons that act as Brønsted acid sites; such sites catalyze the hydration of propene to isopropanol and of PO to diols and their dehydrogenation to 1-propenol and propanal (Scheme 1). The presence of Cs led to about a two-fold increase in PO formation rates (factors of 2.0 and 2.3 for Cs/Au values of 7 and 12, respectively) and a four-fold increase in acrolein formation rates (by factors of 4.3 and 4.6), consistent with a promotional effect conferred by Cs; yet, the presence of Cs was not essential for the formation of either product, as shown by their formation on the samples with undetectable alkali content.

PO turnover rates on these Cs-impregnated Au/TS-1 samples (up to 14×10^{-5} s^{-1}) remained lower than those reported previously for Cs-promoted Au/TS-1 catalysts prepared by DP methods (660×10^{-5} s^{-1}; 0.20% wt. Au; Cs/Au = 15; 53.6% PO; 473 K; 10 kPa O_2; 10 kPa C_3H_6; 2.5 kPa H_2O; 0.22% conversion [11]), which contained Cs as a result of the use of Cs_2CO_3 as a precipitation agent for Au^{3+} precursors. The introduction of Cs into the Au/TS-1 system in this manner, rather than through the aqueous impregnation of Cs_2CO_3 onto Au/TS-1 having Au domains already in metallic form, may promote intimate Au-Cs contact that could partially account for the larger PO formation rates observed on Au/TS-1 systems prepared by DP rather than the methods in this work.

Highly-dispersed Au clusters ($\ll$ 1 nm in diameter) that are not detected by TEM are exceptionally active for PO formation with either H_2/O_2 or H_2O/O_2 reactants, and plausibly account for measured turnover rates on Au/TS-1 systems [11,15,17,18]. The formation mechanism of Au nanoparticles and the thermal treatments required to remove organic residues in the Au/TS-1 samples reported in the present study (773 K; Section 2.3) may essentially eliminate such sub-nanometer Au domains. Synthetic protocols used previously to prepare Au/TS-1 samples (deposition–precipitation [11] or mechanical grinding [50]) predominantly form Au nanoparticles that decorate external surfaces of TS-1 crystals, but do not involve thermal treatments above 473–573 K; these methods may preserve minority Au species of very small size that are predominantly responsible for measured rates.

It is possible for the methods reported to preserve such small Au domains through the use of O_3 or H_2O_2 as chemical reagents during the removal of synthetic organic residues or through controlled pre-conditioning of such organic residues in inert environments, thus inhibiting the coalescence of intracrystalline Au domains. The relatively modest enhancement in PO formation rates conferred by post-synthetic Cs deposition onto the Au/TS-1 samples prepared in this work (Table 3) seems to indicate that the alkali promotional effect is most pronounced for exceptionally small (<1 nm) Au domains that are much less prevalent in these Au/TS-1 catalysts, but it is not an essential requirement for turnovers to occur. It seems plausible that such cations may, in fact, aid the formation of sub-nanometer Au domains and their migration into TS-1 crystals for materials prepared by deposition–precipitation that often use alkali salts as reagents; in doing so, the role of alkali may influence the number instead of the chemical properties of the Au-based species formed.

The strong effects of Au dispersion on propylene-O_2-H_2O reaction turnover rates, taken together with the modest rates achieved here through the selective confinement of Au nanoclusters within TS-1 crystals, suggest that the proximity between Au nanoclusters and Ti centers is not, of itself, beneficial for the dynamics of purportedly bifunctional routes to PO formation. Thus, it appears that, whether by means of their shorter average distances from Ti centers or because of their unique surface reactivity, sub-nanometer Au domains represent the essential mediators of reactivity. The evidence provided here does not resolve the matter of whether the two required sites (Au and Ti centers) must establish atomic contact, but indicate that mere proximity, created here by encapsulation, is insufficient for high reactivity. We remark, however, that atomic contact would not be required if Au domains would form molecular shuttles of electrophilic O-atoms. In our previous work on Au/TiO_2 systems [10], we ruled out H_2O_2 as the epoxidation shuttle with H_2O/O_2 reactants, based on the highest concentrations allowed by thermodynamics and their collision frequencies with TiO_2 surfaces. Similar arguments would not preclude a role for molecular shuttles derived from propylene-O_2

Table 3
Propylene oxide formation rates on Au/TS-1 doped with Cs_2CO_3 after synthesis.

Alkali Promoter	Cation/Au Molar Ratio	PO TOR (10^{-4} s^{-1})[a]	PO Formation Rate (10^{-10} mol g_{cat}^{-1} s^{-1})[a]	PO/Acrolein Ratio	% Propene Conversion
None	0	0.5	8.1	1.2	0.007
Cs	7	1.2	16.4	0.5	0.02
Cs	12	1.4	18.8	0.6	0.02

[a]PO turnover rate (TOR) or formation rate on Au/TS-1 (with 0.9% wt. Au; $\langle d_{TEM} \rangle$: 3.8 nm) post-synthetically impregnated via incipient wetness by aqueous Cs_2CO_3 and then used in reaction (473 K, 3.7 kPa propylene, 3.7 kPa O_2, 6.0 kPa H_2O, 87.6 kPa He; 60,000 cm^3 $g_{cat}^{-1}h^{-1}$). Turnover rates are defined as the moles of PO formed per unit time normalized by the number of exposed metal surface atoms estimated using particle dispersions derived from TEM (Eq. (2)).

reactants, which may form at the Au function and then deliver electrophilic O-species to TiO_2 centers. Such species may include 3-hydroperoxyprop-1-ene and 3-methyl-1,2-dioxetane, which can likely form on Au surfaces [51], and which would react on Ti centers to give equimolar mixtures of acrolein and PO; such equimolar selectivities are not very dissimilar from those observed on Au/TS-1.

The synthetic protocols developed here are able to selectively confine Au nanoparticles within TS-1 through the novel use of low-temperature crystallization promoted by protozeolitic fragments, thus circumventing the premature decomposition/reduction of ligated Au precursors. These methods intended to bring Au and Ti functions closer together for practical benefits; instead, they demonstrated that very small Au domains appear to be the overarching pre-requisite for high turnover rates. The synthetic techniques, however, are applicable to the encapsulation of metal clusters within other high-Si frameworks (e.g., ZSM-48, ITQ-29) that, as in the case of TS-1, require high crystallization temperatures (443–448 K; [46,52,53]). Such techniques may be further paired with post-synthetic modification by organosilanes to form hydrophobic crystals [54] having encapsulated metal particles, which have shown promise for partial methane oxidation [55]. These methods are also transferable to the incorporation of other cationic precursors that interact with thiol groups in MPS (e.g., Pt^{2+}, Pd^{2+}, Ag^{+}, Ir^{4+}) and mixtures of different cations to form bimetallic nanoparticles. In this context, AuPd nanoparticles confined within TS-1 are of special interest because of their high selectivity in forming H_2O_2 from H_2-O_2 reactants [21,56,57,58]. As such, the contents of this manuscript contribute to matters well beyond the testing of hypotheses of interest for epoxidation by O_2-H_2O reactants on Au/TS-1.

4. Conclusions

Au nanoparticles, monodisperse in size, were encapsulated within TS-1 frameworks via the hydrothermal assembly of TS-1 synthesis gels containing ligand-protected Au^{3+} cations. Significant modifications to established crystallization procedures for TS-1 were required in order to prevent the premature decomposition of Au^{3+} coordination compounds within the synthesis gels without adversely affecting the crystallinity of the TS-1 frameworks formed. Such modifications included the use of a lower crystallization temperature, a longer crystallization time, and the incorporation of TS-1 seed crystals into the synthesis gels. The application of these procedures leads to the assembly of crystalline TS-1 with ligated Au^{3+} species occluded in TS-1 micropores; subsequent oxidative thermal treatments result in the formation of clean Au nanoparticles selectively encapsulated within TS-1 crystallites. These Au/TS-1 systems are poorly active for the formation of propylene oxide (with H_2O/O_2) despite the close proximity between Au and Ti sites required for the in-situ generation of *OOH species that oxidize propylene to form the epoxide – possibly due to high post-treatment temperatures leading to significant sintering of Au particles. Poor catalyst activity could be partly surmounted by shifting the mean Au particle size downward through the use of pyrolytic instead of oxidative post-synthetic treatments, reflecting the size-sensitive nature of propene epoxidation rates on Au particles. The post-synthetic doping of these Au/TS-1 systems by alkali promoters, while beneficial for propylene oxide formation rates, was not a requirement to achieve appreciable epoxidation activity. The synthetic procedures outlined in this work provide guiding principles for the encapsulation of metal species within high-Si zeotype frameworks, which typically require high crystallization temperatures that strongly favor the premature decomposition of ligated metal precursors incorporated into synthesis gels.

Author contributions

T.O., S.I.Z., and E.I. conceived and developed the synthesis technique, and drafted most of the manuscript. T.O. and X.Z. performed all chemical syntheses and the other characterization and catalytic experiments.

Declaration of Competing Interest

The authors declare the following financial interests/personal relationships which may be considered as potential competing interests: [Enrique Iglesia reports financial support was provided by Chevron Energy Technology Co. Trenton Otto reports financial support was provided by Chevron Energy Technology Co. Stacey I Zones reports financial support was provided by Chevron Energy Technology Co. Trenton Otto reports a relationship with Chevron Energy Technology Co that includes: employment and equity or stocks. Stacey I Zones reports a relationship with Chevron Energy Technology Co that includes: employment and equity or stocks. Previously editor-in-chief of the journal - EI].

Acknowledgements

We gratefully acknowledge the generous financial support of the Chevron Energy Technology Co, as well as ancillary research support from a National Science Foundation Fellowship (for TO).

Appendix A. Supplementary material

Supplementary data to this article can be found online at https://doi.org/10.1016/j.jcat.2022.04.002.

References

[1] A. Abad, A. Corma, H. García, Chem. Eur. J. 14 (2008) 212–222.
[2] T. Mallat, A. Baiker, Chem. Rev. 104 (2004) 3037–3058.
[3] G.J. Hutchings, Chem. Commun. (2008) 1148–1164.
[4] C.P. Gordon, H. Engler, A.S. Tragl, M. Plodinec, T. Lunkenbein, A. Berkessel, J.H. Teles, A.-N. Parvulescu, C. Copéret, Nature 586 (2020) 708–713.
[5] J.J. Bravo-Suarez, J. Lu, C.G. Dallos, T. Fujitani, S.T. Oyama, J. Phys. Chem. C 111 (2007) 17427–17436.
[6] T.A.R. Nijhuis, T. Visser, B.M. Weckhuysen, Angew. Chem., Int. Ed. 44 (2005) 1115–1118.
[7] B. Chowdhury, J.J. Bravo-Suarez, N. Mimura, K.K. Bando, S. Tsubota, M. Haruta, J. Phys. Chem. B 110 (2006) 22995–22999.
[8] D. Farrusseng, A. Tuel, New J. Chem. 40 (2016) 3933–3949.
[9] S. Kanungo, D.M. Perez Ferrandez, F.N. d'Angelo, J.C. Schouten, T. Nijhuis, A, J. Catal. 338 (2016) 284–294.
[10] M. Ojeda, E. Iglesia, Chem. Commun. 3 (2009) 352–354.
[11] Perez Ferrandez, D. M.; Fernandez, I. H.; Teley, M. P. G.; de Croon, M. H. J. M.; Schouten, J. C.; Nijhuis, T. A. *J. Catal.* **2015**, *330*, 396–405.
[12] J. Huang, T. Akita, J. Faye, T. Fujitani, T. Takei, M. Haruta, Angew. Chem. Int. Ed. 48 (2009) 7862–7866.
[13] B. Taylor, J. Lauterbach, W.N. Delgass, Catal. Today 123 (2007) 50–58.
[14] W.-S. Lee, M.C. Akatay, E.A. Stach, F.H. Ribeiro, W.N. Delgass, J. Catal. 287 (2012) 178–189.
[15] W.-S. Lee, L.-C. Lai, M.C. Akatay, E.A. Stach, F.H. Ribeiro, W.N. Delgass, J. Catal. 296 (2012) 31–42.
[16] W.-S. Lee, M.C. Akatay, E.A. Stach, F. Ribeiro, W.N. Delgass, J. Catal. 308 (2013) 98–113.
[17] A.M. Joshi, W.N. Delgass, K.T. Thomson, J. Phys. Chem. C 111 (2007) 7841–7844.
[18] Z. Li, J. Zhang, D. Wang, W. Ma, Q. Zhong, J. Phys. Chem. C 121 (2017) 25215–32522.
[19] J. Lu, X. Zhang, J.J. Bravo-Suárez, T. Fujitani, S.T. Oyama, Catal. Today 147 (2009) 186–195.
[20] J. Huang, T. Takei, T. Akita, H. Ohashi, M. Haruta, Appl. Catal. B 95 (2010) 430–438.
[21] Moreno, I.; Dummer, N. F.; Edwards, J. K.; Alhumaimess, M.; Sankar, M.; Sanz, R.; Pizarro, P.; Serrano, D. P.; Hutchings, G. J. *Catal. Sci. Technol.* **2013**, *3*, 2425–2434.
[22] R. Ryoo, S.J. Cho, C. Pak, J.G. Kim, S.K. Ihm, J.Y. Lee, J. Am. Chem. Soc. 114 (1992) 76–82.
[23] T. Otto, S.I. Zones, E. Iglesia, J. Catal. 339 (2016) 195–208.

[24] T. Otto, J.M. Ramallo-Lopez, L.J. Giovanetti, F.G. Requejo, S.I. Zones, E. Iglesia, J. Catal. 342 (2016) 125–137.
[25] M. Choi, Z. Wu, E. Iglesia, J. Am. Chem. Soc. 132 (2010) 9129–9137.
[26] T. Otto, S.I. Zones, E. Iglesia, Microporous Mesoporous Mater. 270 (2018) 10–23.
[27] S. Goel, Z. Wu, S.I. Zones, E. Iglesia, J. Am. Chem. Soc. 134 (2012) 17688–17695.
[28] M. Moliner, J.E. Gabay, C.E. Kliewer, R.T. Carr, J. Guzman, G.L. Casty, P. Serna, A. Corma, J. Am. Chem. Soc. 138 (2016) 15743–15750.
[29] A.J.H.P. van der Pol, J.H.C. van Hooff, Appl. Catal. A 92 (1992) 93–111.
[30] M. Wang, J. Zhou, G. Mao, X. Zheng, Ind. Eng. Chem. Res. 51 (2012) 12730–12738.
[31] T. Otto, S.I. Zones, Y. Hong, E. Iglesia, J. Catal. 356 (2017) 173–185.
[32] Z. Wu, S. Goel, M. Choi, E. Iglesia, J. Catal. 311 (2014) 458–468.
[33] S.G. Bratsch, J. Phys. Chem. Ref. Data 18 (1989) 1–21.
[34] Bergeret, G.; Gallezot, P. In Handbook of Heterogeneous Catalysis; Ertl, G., Knozinger, H., Schuth, F., Weitkamp, J., Eds.; Wiley-VHC: Weinheim, Germany, 2008; pp 738–765.
[35] W. Luo, M. Sankar, A.M. Beale, Q. He, C.J. Kiely, P.C.A. Bruijnincx, B.M. Weckhuysen, Nat. Commun. 6 (2014) 1–10.
[36] D. Burevski, Colloid Polym. Sci. 260 (1982) 623–627.
[37] J. García-Martinez, D. Cazorla-Amorós, A. Linares-Solano, Stud. Surf. Sci. Catal. 128 (2000) 485–494.
[38] P. Kubelka, F. Munk, Z. *Tech. Phys*. 12 (1931) 593–601.
[39] B. Van de Voorde, M. Hezinova, J. Lannoeye, A. Vandekerkhove, B. Marszalek, B. Gil, I. Beurroies, P. Nachtiqall, D. De Vos, Phys. Chem. Chem. Phys. 17 (2015) 10759–10766.
[40] C.M. Baerlocher, Database of Zeolite Structures. http://www.iza-structure.org/databases/, 2017 (accessed February 2018).
[41] Nakagawa, Y.; Dartt, C. Pure Phase Titanium-Containing Zeolite Having MEL Structure, Process for Preparing same, and Oxidation Processes using same as Catalyst. U.S. Patent 5,968,474, Oct 19, 1999.
[42] S. Goel, S.I. Zones, E. Iglesia, Chem. Mater. 27 (2015) 2056–2066.
[43] K. Iyoki, K. Itabashi, T. Okubo, Microporous Mesoporous Mater. 189 (2014) 22–30.
[44] A.A.C. Carabineiro, B.E. Nieuwenhuys, Gold Bull. 42 (2009) 288–301.
[45] T. Venkov, K. Fajerwerg, L. Delannoy, H. Klimev, K. Hadjiivanov, C. Louis, Appl. Catal., A 301 (2006) 106–114.
[46] C.B. Dartt, C.B. Khouw, H.-X. Li, M.E. Davis, Microporous Mater. 2 (1994) 425–437.
[47] G. Xiong, Q. Jia, Y. Cao, L. Liu, Z. Guo, RSC Adv. 7 (2017) 24046–24054.
[48] S. Peng, J.M. McMahon, G.C. Schatz, S.K. Gray, Y. Sun, Proc. Natl. Acad. Sci. U.S.A. 107 (2010) 14530–14534.
[49] S. Chavez, V.G. Rao, S. Linic, Faraday Discuss. (2018), https://doi.org/10.1039/C8FD00143J.
[50] J. Huang, T. Takei, H. Ohashi, M. Haruta, Appl. Catal. A 435–436 (2012) 115–122.
[51] P. Geenen, H.J. Boss, G. Pott, J. Catal. 77 (1982) 499–510.
[52] F. Crea, A. Nastro, J.B. Nagy, R. Aiello, Zeolites 8 (1988) 262–267.
[53] A. Corma, F. Rey, J. Rius, M.J. Sabater, S. Valencia, Nature 431 (2004) 287–290.
[54] M. Aly, M. Saeys, Chem. Catal. 1 (2021) 761–762.
[55] Z. Jin, L. Wang, E. Zuidema, K. Mondal, M. Zhang, J. Zhang, C. Wang, X. Meng, H. Yang, C. Mesters, F.-S. Xiao, Science 367 (2020) 193–197.
[56] J. Pritchard, L. Kesavan, M. Piccinini, Q. He, R. Tiruvalam, N. Dimitratos, J.A. Lopez-Sanchez, A.F. Carley, J.K. Edwards, C.J. Kiely, G.J. Hutchings, Langmuir 26 (2010) 16568–16577.
[57] T. Ricciardulli, S. Gorthy, J.S. Adams, C. Thompson, A.M. Karim, M. Neurock, D. W. Flaherty, J. Am. Chem. Soc. 143 (2021) 5445–5464.
[58] H.W. Lee, E. Jung, G.-H. Han, M.-C. Kim, D. Kim, K.-Y. Lee, S.S. Han, T. Yu, J. Phys. Chem. Lett. 12 (2021) 11098–11105.